CHALMERS

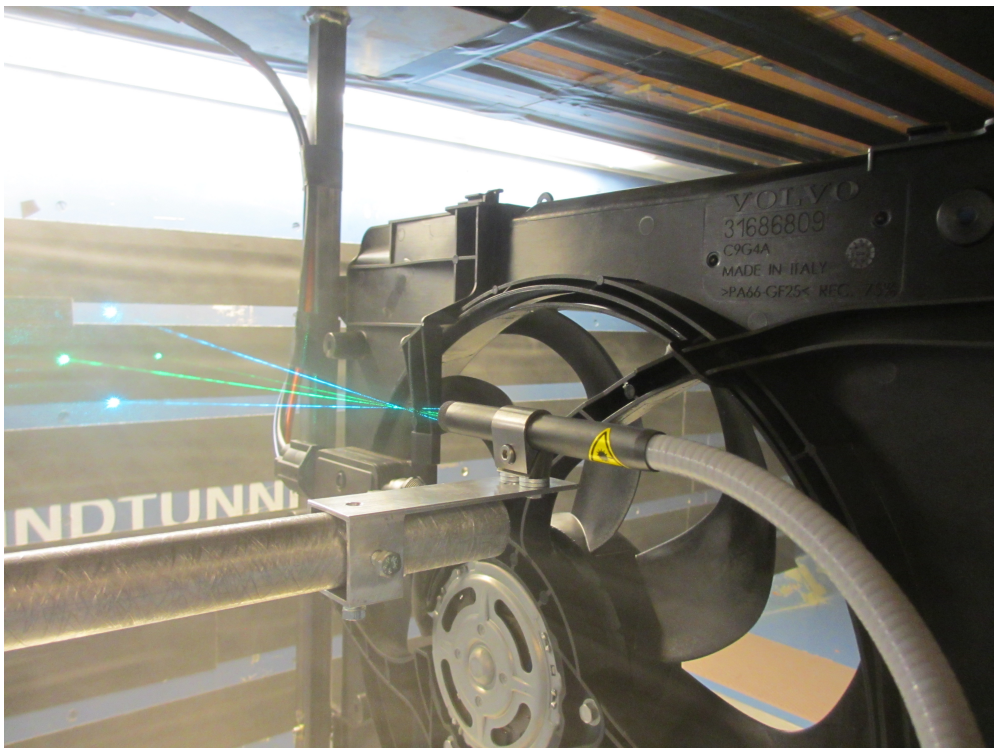

Measurement of Vehicle Cooling Fan Air Flow using Laser Doppler Anemometry

Master's thesis in Applied Mechanics

DAVID ENGLÉN

Department of Mechanics and Maritime Sciences
CHALMERS UNIVERSITY OF TECHNOLOGY
Göteborg, Sweden 2018

MASTER'S THESIS IN APPLIED MECHANICS

Measurement of Vehicle Cooling Fan Air Flow using Laser Doppler Anemometry

DAVID ENGLÉN

Department of Mechanics and Maritime Sciences
Division of Vehicle Engineering and Autonomous Systems
CHALMERS UNIVERSITY OF TECHNOLOGY

Göteborg, Sweden 2018

Measurement of Vehicle Cooling Fan Air Flow using Laser Doppler Anemometry
DAVID ENGLÉN

Master's thesis 2018:50
Department of Mechanics and Maritime Sciences
Division of Vehicle Engineering and Autonomous Systems
Chalmers University of Technology
SE-412 96 Göteborg
Sweden
Telephone: +46 (0)31-772 1000

Cover:
LDA measurement downstream of the investigated automotive cooling fan

Chalmers Reproservice
Göteborg, Sweden 2018

Measurement of Vehicle Cooling Fan Air Flow using Laser Doppler Anemometry
Master's thesis in Applied Mechanics
DAVID ENGLÉN
Department of Mechanics and Maritime Sciences
Division of Vehicle Engineering and Autonomous Systems
Chalmers University of Technology

Abstract

When a combustion engine in a vehicle is operating it generates large amount of heat. Therefore it is crucial to provide cooling in the engine bay to prevent components from overheating. The axial fan in the front of the engine bay is a very import component of the cooling procedure, since it drives fresh air through the heat exchangers into the engine bay. To study the behaviour of the cooling air flow in the engine bay, numerical simulations are commonly used today, but in order to verify and develop numerical tools, physical testing is needed.

In this thesis, LDA has been used to investigate how the actual flow field behaves in the wake of a circular cylinder and the cooling fan used in a Volvo V40. Laser Doppler Anemometry, LDA is a non-intrusive optical technique used for velocity measurements of turbulent and laminar flows. The measurements were performed in the model scale wind tunnel at Volvo Cars. From the cylinder measurements, the performance of the experimental equipment could be confirmed to yield precise results.

The downstream flow behaviour of the fan was investigated for cases with different contributions of wind tunnel velocity and fan rotation speed. Results of the downstream velocity field in all three directions are presented at different distances downstream of the fan. Furthermore, the influence of the mesh resolution on the measured velocity fields is shown and discussed. Lastly, a spectral analysis of the vortex shedding downstream the blade span was performed.

Keywords: Laser Doppler Anemometry, Experimental, Wind Tunnel, Automotive Cooling Fan, Circular Cylinder, Downstream Velocity Field

Preface

This master's thesis work was performed at Volvo Car Corporation, Torslanda, Sweden as the final work in the master's programme Applied Mechanics. The work was carried out during the spring of 2018 at the Division of Vehicle Engineering and Autonomous Systems at Chalmers University of Technology, Sweden. The aim of the thesis was to investigate the downstream flow behaviour of a vehicle cooling fan using Laser Doppler Anemometry.

Acknowledgements

First of all, I would like to thank my supervisor at Volvo Cars, Randi Franzke for giving me the opportunity to do this thesis. Without her support and guidance though out the work this thesis would not have been possible. I would also like to thank Micheal Bolzon, at Volvo Cars, for the practical and theoretical help concerning the measurements. Thanks to my examiner, Simone Sebben for her advice during the work and feedback when planning the project. Finally, I would like to thank the entire team at the Cooling Performance and Heat Management department at Volvo Cars for the kind welcoming and help whenever needed.

Nomenclature

Δf	Doppler Shift
λ	Wavelength
θ	Angle Between Laser Beams
d_f	Fringe Spacing
f_d	Doppler Frequency
f_i	Frequency of Incoming Light
f_s	Frequency of Scattered Light
v_f	Fringe Velocity
v_p	Particle Velocity
v_x	Velocity x-direction
BSA	Burst Spectrum Analyzer
CFD	Computational Fluid Dynamics
LDA	Laser Doppler Anemometry
PWM	Pulse-Width Modulation
RMS	Root Mean Square
RPM	Revolutions Per Minute
Std dev	Standard Deviation

Contents

List of Tables

List of Figures

1 Introduction

In this section the background for this thesis is presented as well as the aim and a specification of the issue under investigation. Finally, the limitations are listed.

1.1 Background

Established procedures for verification in the automotive industry rely heavily on physical testing. These procedures are well tested and fully integrated in the work flow but they require high cost and long preparation time. Therefore, Volvo Cars is interested in the evolution of virtual design to further improve its vehicles, and always integrate the more recent innovations. Virtual design of products consists in using numerical simulations to predict the evolution of a physical system. Coupled with high performance computing, virtual design offers fast and reliable testing of complete vehicles, in particular allowing to identify critical regions. However, in order to develop more reliable numerical tools, a better knowledge of the flow physics inside the engine bay is needed.

In situations when the temperature in the engine bay is rising, cooling is needed to maintain an optimal engine operating climate. To solve the problem of the generated heat and keep a constant temperature in the engine bay a heat exchanger and a fan are used, located behind the grille at the frontal air intake. Increasing engine complexity in combination with a growing interest of aspects as weight and comfort, the space inside the engine bay is getting more and more limited. This causes the need for a good cooling air flow in the engine bay to not overheat the components in this very crowded space and maximize the lifetime of the engine.

With its ability to accurately study flow details in small confined spaces, Laser Doppler Anemometry (LDA) is a good technique for engine bay measurements. It is insensitive to the high temperatures in this area and no measuring sensors that disturb the flow in the measurement point are needed. The technique can be used to characterize the air flow and recirculation regions in order to increase the cooling efficiency.

1.2 Aim

The aim of the thesis is to provide a better understanding of the flow phenomena downstream the engine bay cooling fan. Further, investigate if LDA is a good method for this kind of flow field investigations and can work as a verification method for CFD.

1.3 Specification of issue under investigation

Since the flow in the engine bay often is unsteady and highly turbulent it can be hard to capture the real physics of the flow with numerical tools. Therefore, in this thesis it will be investigated how the actual flow behaves downstream of the cooling fan in the engine bay. This will help to develop numerical tools that give accurate results in an appropriate lead time.

These measurements are performed in the model-scale wind tunnel at Volvo Cars using Laser Doppler Anemometry. The results can be used to compare with corresponding CFD calculations. In order to achieve accurate results, initially the measuring equipment has to be properly aligned and installed. To get familiarized with the method and make sure that the measuring equipment works well with the choice of seeding particles, measurements on a circular cylinder are first performed before moving on to the fan investigation.

1.4 Limitations

This thesis only focuses on physical testing and evaluation of the results in order to compare with numerical methods, thus no CFD calculations will be performed since this does not fit within the timeline of the project. However, to make sure that physical results were obtained, a comparison to existing CFD data of the same geometry is performed.

The seeding particles in the air flow is limited to smoke created by a smoke machine.

The measurements are performed on the flow around the Volvo V40 fan used for cooling of the engine bay and not the entire engine bay flow since this would be very difficult in the model-scale wind tunnel.

2 Theory

This chapter explains the theory behind engine cooling and Laser Doppler Anemometry. Finally a literature study of previous work in the area is presented.

2.1 Engine Cooling

The internal combustion engine of a vehicle operates most efficiently at relatively high temperatures. The engine combustion process will however generate very high temperatures that quickly cause devastating damage on the engine if not controlled. The purpose of the cooling system is to quickly let the engine reach optimum temperature and maintain this temperature during operation by dissipating the excess heat.

The cooling system is located at the front of the engine bay behind the grill and mainly consists of a radiator to cool the liquid coolant, one or two fans to make sure that adequate airflow through the heat exchangers is obtained, a thermostat to keep desired temperature and a pump to circulate the coolant. When the liquid coolant circulates through passages of the engine it absorbs heat. The heated fluid then flow through the radiator tubes where it is cooled by the airflow entering through the grill at the front of the car. The coolant then continue to circulate with help of the pump and the system is controlled by the thermostat. A typical engine colling system is shown in Figure 2.1 This process cools the engine but keeps a high enough temperature for an optimal engine operating condition, resulting in a longer lifetime of the engine components and less pollution emissions.

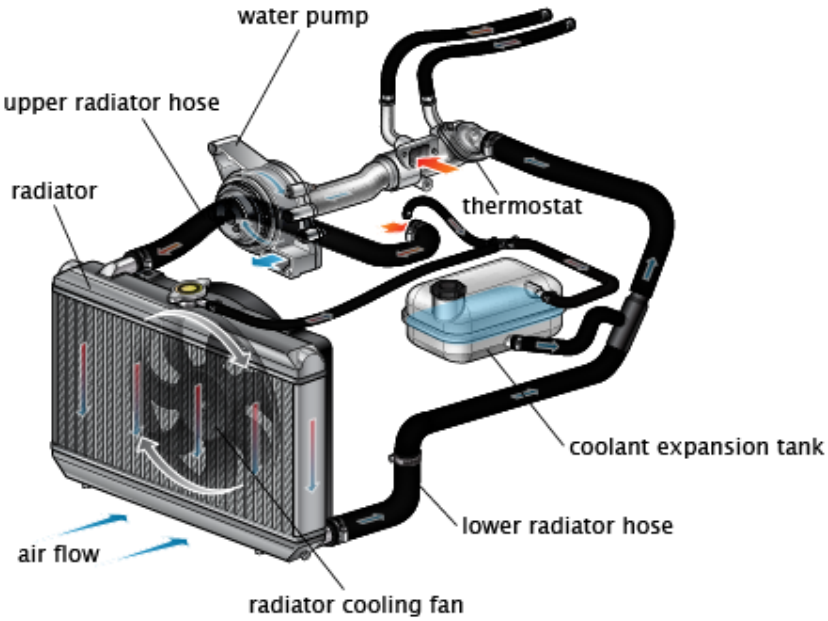

Figure 2.1: *Cooling system, source [1]*

2.2 Cooling Fan

When driving with high speed there is a natural inflow of surrounding air through the grille, following the relative velocity between the car and ambient air, at the front of the car to cool the engine. But in situations when for example the car is moving at low speed or while the car is running idle, the natural incoming airflow cannot provide enough cooling. To solve this a radiator cooling fan is used. On modern vehicles this is normally one or two electric driven fans placed behind the radiator. When the temperatures in the engine bay is increasing the fan starts to run and forces a higher airflow through the radiator to cool the coolant and direct the flow in the engine bay.

If the car has an air conditioning system a second heat exchanger, called condenser, is located in front of the radiator. The condenser is smaller than the radiator but constructed in a similar way. Since the condenser, just like the radiator, needs to be cooled by airflow it also makes use of the fan. The purpose of the condenser is to release heat from the A/C refrigerant by cooling the hot compressed refrigerant gas into a high pressure liquid in order to keep a good climate in the coupe.

2.3 Model-scale Wind Tunnel

The measurements were performed in the model-scale wind tunnel at Volvo Cars. The wind tunnel is a $1/5^{\text{th}}$ prototype of the full-scale wind tunnel and has a maximum wind velocity of about 55 m/s (200 km/h) mainly used for aerodynamic testing. It is of closed circuit type and the test section is equipped with slotted walls to reduce the interference of the walls during measurements. The test section floor has a turntable to be able to rotate the studied object in order to account for side load wind effects. At the test section the wind tunnel has a width of 1.32 m and a height of 0.82 m giving a cross section area of 1.08 m^2. Just upstream of the test section there is a boundary layer suction in order to reduce the boundary layer.

2.4 Laser Doppler Anemometry

Nowadays, to study complex flows there is a wide use of numerical methods (CFD), but its applicability and reliability in many cases still needs to be complemented by experimental investigations. A well known technique that has been used since the mid 60s to study turbulent and laminar flows is Laser Doppler Anemometry, LDA. Over the decades, following the optical and electrical evolution, the method has been greatly improved and is today an accurate technique useful in a wide range of applications, such as aerodynamic testing and turbulent research.

To understand the working principle of LDA some theory will first be presented.

2.4.1 Turbulent Flows

In most industrial fluid dynamic applications the flow is turbulent. Turbulent flows are always three-dimensional and unsteady. The fluid velocity field of turbulent flows are

strongly fluctuating and irregular in both position and time. Turbulent flow is characterized by a large range of scales. The energy generated by the largest turbulent scales in the flow are transferred through the spectrum of scales to the smallest scale structures, the Kolmogorov length scales, where the kinetic energy is dissipated to thermal energy.
Due to the random and chaotic behavior of turbulent flows it is very computational costly to resolve the scales and therefore turbulence is most often modelled, lowering the computational load but with the drawback of introducing inaccuracies. Therefore experimental methods as LDA is often used to study turbulent flows and measure the irregular fluctuating velocities.

2.4.2 LDA Principle

Laser Doppler Anemometry, also known as Laser Doppler Velocimetry, is an optical method that combines the optical Doppler effect for measurements of velocity in a single point. It can be used to obtain velocity components in one-, two- or three dimensions. In wind tunnel testing, LDA is commonly used to study aerodynamics around an object. Some applicable objectives are reducing drag, minimizing wind noise, reducing energy consumption and to validate numerical simulations.

LDA is a non-intrusive technique meaning that no flow disturbing equipment must be used in the measurement point, and except for the initial setup and alignment of the equipment, there is no need for pre-calibration before measurement. Another advantage of the method is the independence of thermophysical properties of the fluid thus the applicability to measure in harsh environments with for example high temperature and pressure. Also, a wide range of velocities can be measured, from m/s – km/s. However, the method has some drawbacks as well. The equipment needed is expensive and the medium has to be transparent with dispersed seeding particles. It is a point-wise measurement technique and can therefore be very time consuming to get a full picture of the flow field compared to Particle Image Velocimetry. In LDA measurements the probe need to have optical access to the investigated target and velocity bias effects must be dealt with. Velocity bias is a common problem in LDA measurements of turbulent flows and is a consequence of that the sampling rate of velocity is not continuous. More precisely that, large magnitude velocities are proportionally sampled more frequently than small magnitude velocities and therefore leads to a non-equidistant time between two consecutive velocities. This sample shift of mean velocities towards the higher value is called velocity bias.

2.4.3 Doppler Effect

Light propagation is, according to electromagnetic theory, radiating electromagnetic waves oscillating perpendicular to each other in the direction of the wave propagation.

The light propagation velocity is defined as:

$$c = f * \lambda \tag{2.1}$$

Where the wavelength λ is the distance between two crests (or two troughs) and the frequency f is the number of waves passing a fixed point per unit time.

Light from a moving object will appear to have different wavelength depending on the motion relative to the source and observer. More specifically the electromagnetic waves emitted from a moving object will be compressed in the moving direction and expanded in the opposite direction giving rise to a change in wave frequency, visualized in Figure 2.2. Therefore the wavelength will decrease and frequency increase in the forward moving direction and vice versa in the opposite direction. This change of light waves received by a stationary observer form a moving emitter is known as Doppler effect or Doppler shift, first described in 1842 by the Austrian physicist Christian Doppler [2].

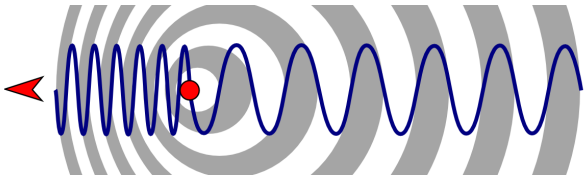

Figure 2.2: *Doppler effect*

In an LDA system, the Doppler effect is exerted as laser light from two intersecting beams, from a fixed laser source, is reflected on moving particles dispersed in the fluid and received by stationary optics.

The frequency of the scattered light observed by the stationary receiving optics can be formulated as

$$f_s = f_i \frac{1 - (e_i v_p / c)}{1 - (e_s v_p / c)} \tag{2.2}$$

where f_i is the frequency of the incoming light, e_i and e_s is unit vectors describing the incoming light from the laser source and the scattered light in the direction of the receiving optics respectively, v_p is the particle velocity and c the speed of light.

When the particle velocity is much smaller than the speed of light, $|v_p| << c$ (which is the case for practically all flows) this expression can be linearized to

$$f_s \approx f_i\big(1 + \frac{v_p}{c}(e_s - e_i)\big) = f_i + f_i \frac{v_p}{c}(e_s - e_i) = f_i + \Delta f \tag{2.3}$$

By measuring the Doppler shift Δf, the particle velocity, as the only unknown, can be obtained.

2.4.4 Configuration

In this study a dual beam fringe model LDA system is used and is the technique described below.

The configuration consists of a continuous laser source and transmitting optics that splits the laser into two parallel beams that in the probe is deflected to an intersection point creating the measurement volume. The laser and transmitter are aligned and mounted on a rigid bench. By using seeding particles in the air flow, light from particles passing through the beam intersection will be reflected to the receiving optics. A photo-multiplier, or photo-detector, then converts the varying light intensity to an electrical frequency signal proportional to the particle velocity. The fast response time of electronic signals in combination with a very small measuring volume gives the method a high temporal- and spatial resolution [3, 4].

Figure 2.3 shows the LDA set-up used in this study, where the laser with belonging adjustment control can be seen to the left, the transmitter to the right and the photo-multipliers at the bottom.

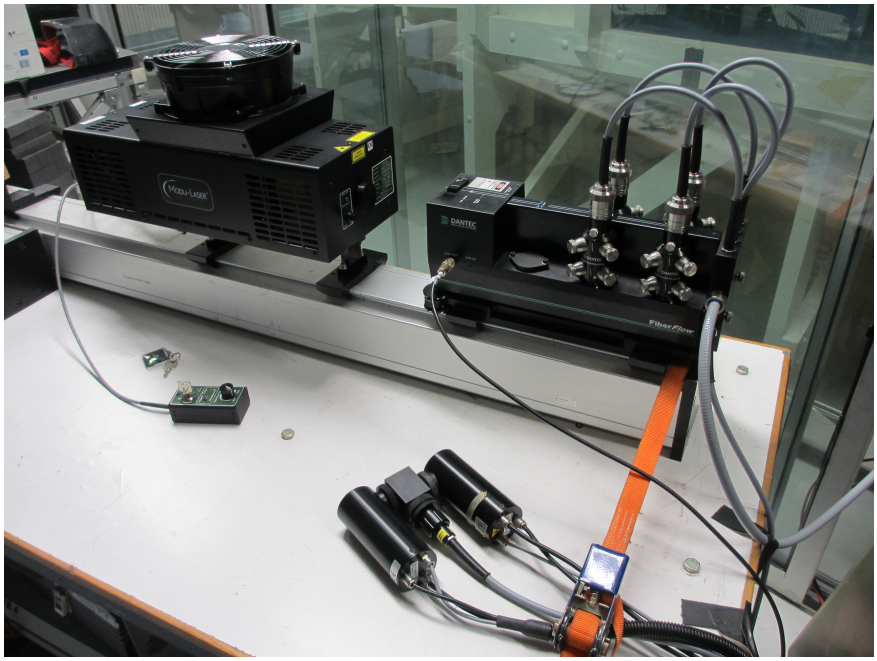

Figure 2.3: *LDA configuration*

Laser Source

In most LDA applications the light source is an argon-ion laser where the radiation energy is created by a gas of argon atoms maintained at the ion state. The emitted beam contains violet, blue and green light with wavelengths of 476.5 nm, 488 nm and 514.5 nm respective which can be used to measure the velocity in three different directions. The laser used in this investigation is a solid state laser providing two different wavelengths, 488 nm and 514.5 nm.

Transmitter including Bragg Cell and Fiber Manipulators

The transmitter consists of a beam splitter, Bragg cell and mirrors with a main purpose to split the beams by color and introduce a frequency shift to one of the beams. For the dual beam technique, a particle crossing the measurement volume will give the same signal as a particle moving in the opposite direction. To solve this issue a Bragg cell is used.

A Bragg cell is an optical device used to split the laser beam into two beams with equal intensity but different frequency so that the directional ambiguity is removed. Without the frequency shift, the beams have equal frequency and it would therefore not be possible for the receiver to detect the direction of the flow.
The Bragg cell is a normally a glass plate with a piezoelectric transducer on one side connected to a oscillator producing an acoustic wave propagating through the plate. The opposite side of the Bragg cell is equipped with an absorber reducing the acoustic waves. As the incoming laser beam interfere with the acoustic waves it will diffract and a frequency

shift will be introduced to one of the beams. By tilting the Bragg cell in a specific angle and adjusting the electric signal to cause a vibration of a sinusoid, the light will be reflected from the flat acoustic waves with a high deflect efficiency, as shown in Figure 2.4 [5, 6].

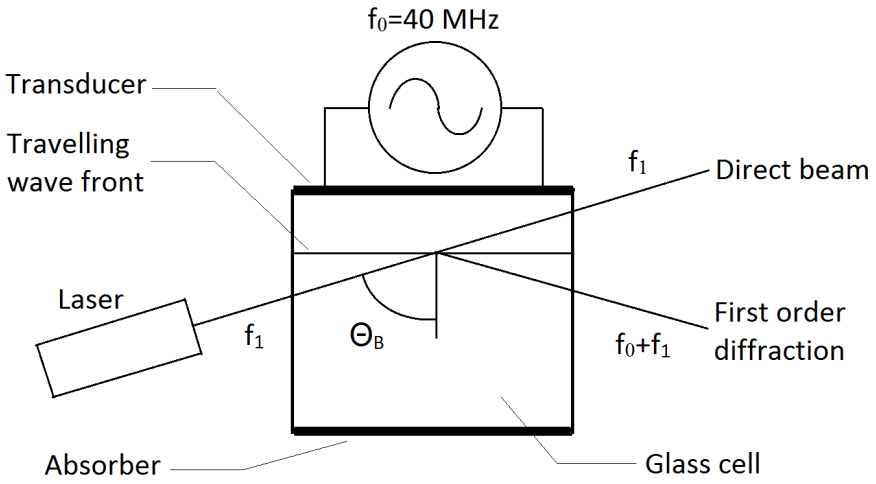

Figure 2.4: *Bragg cell*

By introducing the constant shift of frequency for one of the two split beams, positive and negative velocity directions will generate unique values of detected frequency. With the frequency shift added, the measuring fringe pattern, described below, will no longer be fixed but moving with a constant velocity ($v_f = f_0 * d_f$). So as long as the particle velocity cause a frequency larger than the negative value of the added frequency shift, a positive Doppler frequency will be obtained. A stationary particle will therefore generate a signal frequency equal to the added frequency shift. By measuring if the frequency increases or decreases in response to the moving particle the direction of the flow can be determined.

Scatter frequency from beam 1 is calculated as

$$f_{s1} = f_i\big(1 + \frac{v_p}{c}(e_s - e_{i1})\big) \tag{2.4}$$

Scatter frequency of beam 2 with introduced frequency shift

$$f_{s2} = (f_i + f_0)\big(1 + \frac{v_p}{c}(e_s - e_{i2})\big) \tag{2.5}$$

Now the Doppler frequency can be formulated as a combination of the two beams

$$\begin{aligned} f_d &= f_{s2} - f_{s1} \\ &= (f_i + f_0)\big(1 + \frac{v_p}{c}(e_s - e_{i2})\big) - f_i\big(1 + \frac{v_p}{c}(e_s - e_{i1})\big) \\ &= f_0 + (f_i + f_0)\frac{v_p}{c}(e_s - e_{i2}) - f_i\frac{v_p}{c}(e_s - e_{i1}) \\ &= f_0 + f_i\frac{v_p}{c}(e_{i1} - e_{i2}) + f_0\frac{v_p}{c}(e_s - e_{i2}) \\ &= f_0 + \frac{2sin(\theta/2)}{\lambda}v_x + f_0\frac{v_p}{c}(e_s - e_{i2}) \end{aligned} \tag{2.6}$$

where v_x is the velocity in x-direction. The last term is negligible since the speed of sound

is much larger than the particle velocity

$$\Rightarrow f_d \approx f_0 + \frac{2sin(\theta/2)}{\lambda} v_x \tag{2.7}$$

The Bragg cell used in a 2D LDA system adds a frequency shift to one of the green and one of the blue beams. To guide the beams from the transmitter to the optical fibres connecting to the probe, so-called manipulators are used.

The manipulators are equipped with adjustment screws to direct and centre the laser beams to the optical fibre core so that maximum light is transmitted to the probe. One manipulator is needed for each beam, thus for a 1D measurement two manipulators are required, for 2D four manipulators and for 3D six manipulators.

Probe and Measurement Volume

With fiber optics the beams are sent from the transmitter to an optical probe. The optical probe has a convex lens that focus the beam intersection forming the measurement volume. With the backscatter LDA technique, explained below in the *Light Scattering* section, the probe is also used as a receiver of the light scattered from the particles passing through the measurement volume. For this reason the probe is equipped with a second lens to focus the captured light to a multimode fibre cable acting as a spatial filter to increase the quality of the laser light. The difference between the multimode fibre cable transmitting the scattered light and the single mode fibres used for the laser beams is that multimode fibres has a larger core allowing multiple modes of light to propagate. With a higher amount of light reflections in the core, more data can pass through at a given time but at the expense of a reduced signal strength over long distances. Cables with single mode fiber optics has a core with a smaller diameter that allows less light to propagate but with the possibility for the signal to travel further.

There are several different probe sizes available depending on the objective of the measurement. In this study a 2D cylindrical probe with a diameter of 14 mm and a length of 116 mm is used. The beam intersection is located 50 mm in front of the focal lens. The benefits of a small probe is its applicability in constrained places and the low disturbance when placed directly in the flow. The portability of a small probe making it appropriate for mounting on a traverse to easily select measurement positions. With a 2D probe the laser beam will first be split into two beams with different wavelength in the transmitter. Then both beams are split again adding a frequency shift to one of the beams before all four beams, two blue and two green, are guided through fibre optics to the probe.

It is mentioned above that LDA is a single point meassurement technique which is not completely true as the measurement "point" really is a small volume. The measurement volume consists of a pattern of bright and dark parallel planes, with high and low intensity, called fringes. Since the intersecting beams origin from the same source they have equal intensity and waveform. Therefore when the beams overlap, the light will cancel and complement each other in different regions forming the fringe pattern, shown in Figure 2.5.

It is when the particle passes a bright fringe light will be reflected back to the receiving optics. This burst signal is recorded as a frequency by the photo-multiplier with an amplitude altering depending on the fringe spacing.

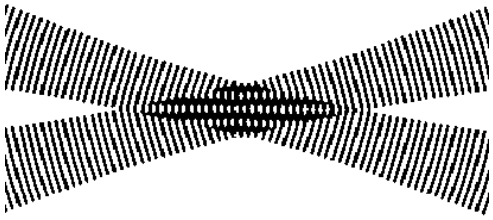

Figure 2.5: *Fringe pattern, source [7]*

Because the laser beam has a Gaussian distribution in nature the fringe pattern will also be characterized by a Gaussian distribution. Following this intensity distribution in all three directions the measurement volume will have an ellipsoidal shape. A 2D probe with four illuminating beams, as used in this study, produces two fringe patterns perpendicular to each other.

When performing LDA measurements it is important that the intersection of the beams occur at the beam waist, which is the smallest cross section of the beam occurring due to that the deviation from the rectilinear light propagation increases with decreasing beam radius. Then, due to that the wave fronts are plane at the beam waist the fringes will be parallel. If the beams are not properly aligned the measurement volume will not occur at the beam waist and the wave fronts will instead be curved resulting in a nonparallel pattern of fringes. Then the measured Doppler frequency will be dependent on the particle position in the measuring volume and no longer proportional to the particle velocity.

Light Scattering

The Lorentz-Mie theory states that the light in the dual beam fringe model is scattered in all directions at once. Thus, the position of the receiving optics do not have any influence on the detected frequency, it will only impact the strength of the signal.

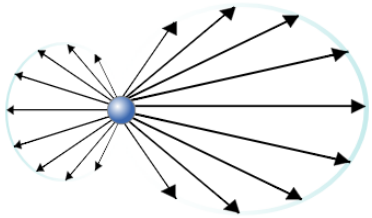

Figure 2.6: *Mie scattering of particle*

The scattered light can be collected in a wide angle with a lens and focused at the photo-multiplier. Two frequently used techniques to receive scattered light is forward scatter and backward scatter. With the forward scatter LDA method the receiving optics are placed opposite to the transmitting optics. This method is preferred when the Doppler signal is weak since the intensity of the scattered light is highest in the forward direction. But with this method the receiving optics must always be directly focused on the measurement volume and is therefore a very cumbersome process when measuring several different positions in the flow. The forward scatter method also needs to have optical access from both sides of the measured point. The today more commonly applied

method is backscatter where the receiving optics is housed in the probe, as explained above, obtaining the light scattered backwards. A backscatter LDA system for measurement of one velocity component is illustrated in Figure 2.7. Even though smaller amount of light is scattered in backward direction the advanced optics today can efficiently measure weaker signals. The main reason for the popularity of this method is that the receiving optics is placed in the probe and is therefore always automatically focused of the measuring volume, removing the need for time-consuming alignment. Also, this method only requires optical access to the measuring position from one side.

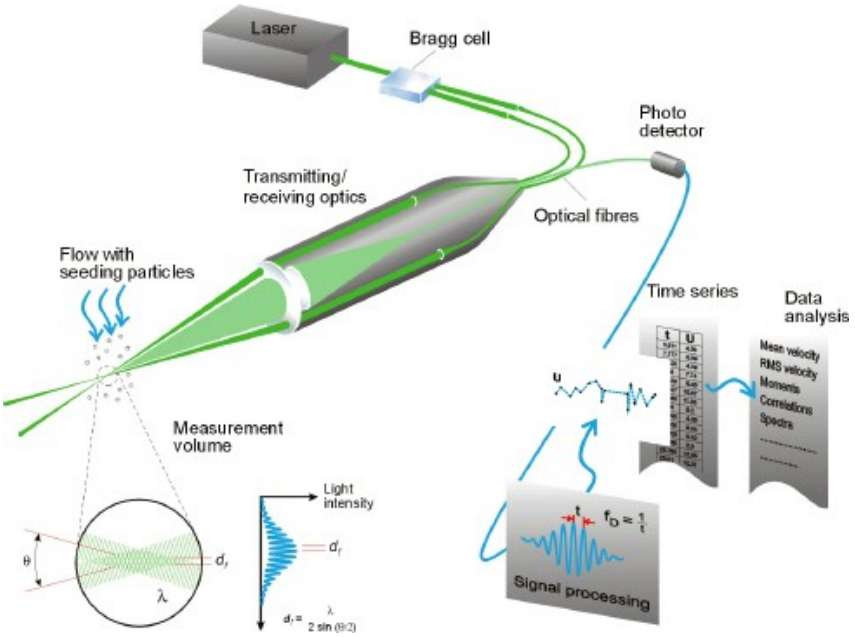

Figure 2.7: *Schematic of a 1D backscatter LDA system, source [8]*

Seeding

With LDA it is not the velocity of the flow that is measured it is the velocity of the particles suspended in the flow. These particles are called seeding particles and are a very important part of LDA measurements. The temporal resolution of the method is usually limited by the concentration of seeding of particles rather than the measuring equipment. The size of the seeding particles must be small enough to completely follow the flow, in order to capture the fluctuations, but big enough to scatter back adequate amount of light. Using too large particles would lead to an uneven spatial resolution due to that a single particle would cover a large part of a fringe, giving unreliable results. Another important aspect of the seeding is the concentration of particles in the fluid, the rate of signals depends on the amount of particles passing in the measurement volume.
Common materials for seeding particles in LDA experiments in air flows are glycol, glycerine, silicone oil, silicon dioxide, aluminum oxide and water.

2.4.5 Data Processing

The output from LDA measurements is in form of filtered electrical sinusoidal signals from where the fluctuating velocity of the turbulent flow can be calculated as shown below.

The Doppler frequency, f_d, is the intensity of reflected light from the fluctuating particles and is proportional to the absolute value of the particle velocity in x-direction. The x-direction is referred to as the direction perpendicular to the optical axis of the transmitting optics, i.e. the wind tunnel flow direction.

The distance between fringes, d_f can be expressed as:

$$d_f = \frac{\lambda}{2sin(\theta/2)} \tag{2.8}$$

where λ is the light wavelength and θ is the angle between the laser beams.

By relating the time (Doppler frequency) to the distance travelled (fringe spacing) one can get an expression for the x-component of the velocity:

$$v_x = d_f * f_d = \frac{\lambda}{2sin(\theta/2)} * f_d \tag{2.9}$$

Which is a linear relation between the Doppler frequency and the particle velocity in x-direction. This can similarly be done for the other velocity components.

By using a two-component probe or by combining two probes, that uses lasers with different wavelength, one can obtain velocity components in multiple directions.

2.4.6 BSA Software

The BSA (Burst Spectrum Analyzer) software is provided by Dantec Dynamics and is used for analysis of LDA measurements. The software operates together with the BSA processor and deals with everything from initialization of measurements to analysis and display of the acquired results.

The software has several build-in tools for analysis of LDA measurements. It is possible to directly obtain plots and values for different time based information as arrival time, transit time (signal duration i.e. the total burst time) and time averaged information as mean- and root-mean-square (RMS) velocity. The software can also show turbulence intensity, validation rate at each position from the readings of the burst spectrum analyzer and anode current, which is a measure of light intensity from the photo-multiplier output current.

In the BSA software there are two possible options to remove velocity bias. One way is to use a *Dead Time mode* in which the time axis is divided into intervals to avoid oversampling the velocity information. To get statistically independent samples with this method the integral time-scale first needs to be estimated so that the dead-time interval can be set accordingly. *Dead Time mode* is useful when moments of the velocity distribution is wanted.

The other alternative is to use the *Burst mode* with the setting for transit time weighting. Transit time weighting assumes that the flow in the measurement volume is uniform and is recommended for flows with spatially homogeneous seeding.

Then the weighting factor, η_i is set to:

$$\eta_i = \frac{t_i}{\sum_{j=0}^{N-1} t_j} \tag{2.10}$$

where N is the number of velocity samples, t_i the transit time of the i^{th} seeding particle passing through the measuring volume.

The *Burst mode* measures every detected burst giving information about the arrival time, transit time and velocity components. This mode is normally used when the signal from the seeding particles is discrete bursts and when a high temporal resolution is required, e.g. for rotating machinery. Thus the *Burst mode* is used throughout in this study.

2.4.7 Traverse System

By mounting the laser probe on a traverse system in the wind tunnel, detailed information about the velocity field around an object can be obtained. To get a precise space mapping of the fluid velocity could require hundreds maybe even thousands measurement points in the flow. The traverse system in the wind tunnel consists of two motors allowing for movement in y- and z-direction. The movement of the traverse is done by the BSA software via a CNC controller. This gives the possibility to generate a mesh of positions in the software to get a automatic movement pattern of the traverse. If desired to study different areas of the flow with varying mesh resolution it is possible to divide the flow into sub-regions with its own set of traverse properties.

2.5 Literature Study

There has been done several measurement studies on engine bay flow. Some previous work done within the field is presented below.

LDA measurements to study the effects of engine blockage for the flow induced by the cooling fan were investigated in [9]. The measurements were performed in a simplified model of the engine compartment containing an air inlet grille, the cooling module and a box representing the engine. The LDA configuration measured two velocity components, streamwise and vertical cross-stream direction, in a plane normal to the flow. Different blockage distances were investigated for two different fan rotational speeds, 1400 and 2800 rpm. These speeds correspond to conventional operation conditions. The study showed that the fan induced flow behaves different if the fan is studied alone or with blockage. With increasing distance between the cooling unit and engine block an increased flow through the radiator was observed. The spacing also have an impact on the axial and vertical velocity components both in size and form. The air flow rate through the heat exchangers increases with increasing blockage distance. Most sensitive to spacing distance is the vertical cross-stream velocity component where the perturbing blockage effect on the flow remains in a higher manner with increasing spacing compared to the streamwise velocity component.

In [10] measurements using hot wire on three different types of axial fans; backward swept, radial and forward swept blades were conducted. The measurements were performed downstream of the fan with the purpose to show the unsteady velocity behavior of the flow field induced by different fan models. The forward swept fan showed the best performance in the aspect of lowest noise and perturbed wake structure. The most interesting region is at the tip of the blades and at midspan where the radial velocity component is high.

Measurements of a low-pressure axial fan in an anechoic test chamber with absorbing walls, ceiling and floor were investigated in [11]. The fan was mounted in a short convergent-divergent duct, driven by a motor outside of the duct. LDA was used to study the flow field in three-dimensions on both the suction and pressure side of the fan, further the fan characteristic curves, wall pressure fluctuations and sound field and was investigated. On the pressure side of the fan the highest meridional velocity was obtained at around 4/5 radius from the fan axis, with a small decrease towards the hub and a strong decrease towards the blade tips near the duct wall. The radial component stays rather constant over the blade span, with the exception of close to the hub where a region with reversed flow was observed. The turbulent kinetic energy was highest at the hub and blade tips.

An investigation of the downstream blockage effect on axial fans in a engine bay test rig and in a plenum chamber with a five beam laser probe obtaining all three velocity components were performed in [12]. Two fans were tested, a low-pressure fan and a conventional high pressure fan. The test showed that the pressure loss increases with decreasing blockage spacing and increasing flow rate. Since the low-pressure fan has a higher flow rate at operation point a smaller pressure loss was observed than for the high pressure fan. From the LDA velocity measurements it could be concluded that the downstream blockage caused a reduced flow rate through the fan. It also increased the reversed flow at hub and forced a higher radial flow along the blade span. The highest radial flow under blockage appeared for the low-pressure fan, again following the higher operating flow rate.

In this study only the fan is investigated and no blockage accounted for. It is clear from literature study that the flow will be very different in these two cases as the blockage cause a reduced flow rate. But, since the main goal of this thesis is not to get full prediction of the engine bay flow, it is more suitable and less time consuming to investigate the fan separately. Similar to [9], fan rotational speeds of 1400 and 2800 rpm are used in this study.

3 Methodology

The chapter presents the methodology of this study, first for the cylinder measurements and then for the fan measurements.

3.1 Cylinder Wake Measurements

To test the measurement equipment as well as the execution procedure, measurements were initially preformed on a simple geometry. The results could then be compared with documented ones to make sure that accurate results are obtained.

A circular cylinder was chosen to be investigated since this is a widely tested geometry with many documented results obtained by different measurement techniques. To be able to make an accurate validation of the results, experiments performed with similar turbulence intensity , blockage ratio , geometry of the cylinder and Reynolds number were used. A cylinder is a bluff body, that due to its shape, is characterized by a flow separation over a substantial part of the surface forming a wake behind the body.

By measuring the fluctuating velocities in the wake of the cylinder the obtained results can be compared with for example mean- and root mean squared velocities in different directions and study how the Strouhal number varies with Reynolds number.

A circular hollow steel cylinder was studied with an outer diameter of 25 mm, a wall thickness of 2 mm and a length of 810 mm giving an aspect ratio of about 32. In one of the cylinder ends a circular steel plate was welded in order to be able to vertically mount the cylinder to the wind tunnel ceiling with screws. Since relatively low wind velocities were studied the cylinder was not expected to need a rigid mounting at the opposite end as well and was just supported by tape between the floor and cylinder to minimize vibrations. This setup gave a blockage ratio of 2 % and can be seen in Figure 3.1. For the specifications of the wind tunnel see Section 2.3.

Figure 3.1: *Set-up for cylinder wake measurements*

The origin of the coordinate system was set at the mid-span position of the cylinder axis with x-direction representing the streamwise, y-direction the horizontal cross-stream and z direction the vertical cross-stream direction.

The LDA measurements were performed at mid-span position of the cylinder with the probe mounted in a horizontal direction normal to the air flow in the wind tunnel, giving velocity components in the x- and z-direction. To measure the velocity component in streamwise- and spanwise direction the green laser (wavelength of 514.5 nm) and blue laser (488 nm) were used respectively. The cylinder was placed a bit off the streamwise centerline of the wind tunnel but still over 50 cm from the nearest wind tunnel wall, so that the interference from the walls could be considered negligible. By traversing the probe across the wake (y-direction) at different distances downstream of the cylinder, the wake structure could be studied.

The measurements were performed across the wake, in y-direction, at 1, 2 and 4 diameters downstream of the cylinder. At each downstream distance four different Reynolds numbers were tested, 8000, 15000, 20000 and 30000 corresponding to freestream velocities of 4.82, 9.04, 12.05 and 18.07 m/s respectively. The wake centerline could be located as the position where the lowest velocities were obtained and the particle count reached a minimum. Acquired values of the mean-, RMS velocities and Strouhal number could then be compared with corresponding values from other studies [13, 14].

The measurements of the velocities along the wake centerline were performed two times so that an averaged value could be calculated, which reduces the uncertainty of the measured velocities. To get results that correlate to the values used for comparison, the measuring distance downstream of the cylinder was scaled with the cylinder diameter and velocities with the free stream velocity. The free stream velocity was determined from measurements at a distance of 20 diameters upstream of the cylinder.

Smoke was generated by a portable smoke machine that was placed downstream of the cylinder and controlled by a remote controller. Similar conditions as in the compared work were aimed for with a particle count of 10000 and data rate of 1000 Hz in x-direction and a count of 5000 particles and data rate of 500 Hz in z-direction. But these values varied much since the measuring points near the wake centerline could not capture as many particles as further aside towards the free stream. The *Burst mode* was used and transit time weighting was applied to the data in order to remove velocity bias effects.

At each measurement position, the velocities of all particles passing the measurement volume were obtained. These time dependent fluctuating velocities could then be converted to a frequency using a fast Fourier transform (FFT). But first the values of the velocities had to be interpolated since the time between measurements of different particle velocities varied and the FFT needs to have a equidistant time spacing. So, the random time sampled data needed to be reconstructed to a sequence of values with equal time intervals, as shown in Figure 3.2. The resulting evenly spaced sequence can then undergo the usual FFT treatment. The linear interpolation and FFT was done in Matlab.

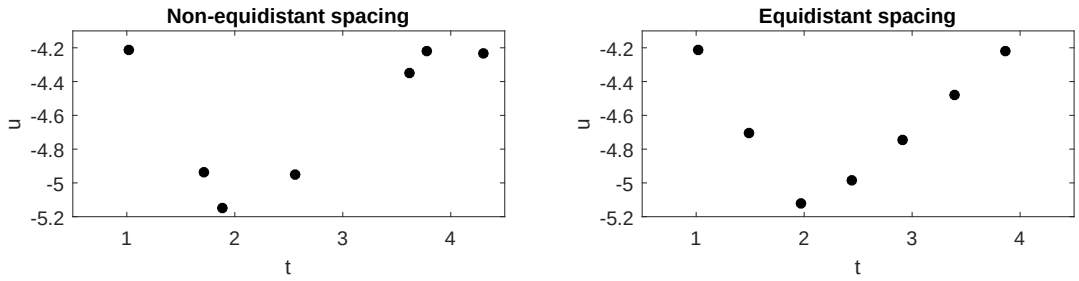

Figure 3.2: *Non-equidistant time spacing (left) and equidistant time spacing (right)*

By taking the value of the frequency at the peak in amplitude, which should correspond to the maximum vortex shedding, the Strouhal number can be calculated as:

$$St = f_s D / U_0 \tag{3.1}$$

where f_s is the shedding frequency, D the cylinder diameter and U_0 the free-stream velocity.

The Strouhal number is a measure of the dominant frequency shedding and is a commonly used parameter for unsteady flows, normally plotted as a function of Re-number. The cylinder measurements were performed in the sub-critical regime (Re=300-150000) where the boundary layer separation occur about 80 degrees downstream of the stagnation point causing a fully turbulent vortex street. In this region the Strouhal number is usually around 0.2 for a circular cylinder [14].

No boundary layer suction was used in the wind tunnel since it was not expected to have an influence at midspan of the cylinder about 410 mm above the floor. For lower wind velocities the air flow in the wind tunnel has a unsteady behaviour with some recirculation, therefore only freestream velocities above 4 m/s were used to remove this source of uncertainty.

3.2 Fan Measurements

The fan investigated in this study is the axial electric cooling fan used in Volvo V40. The entire fan including the shroud and the flaps was mounted in the tunnel but focus was on the downstream area of the rotating fan part.

3.2.1 Experimental Setup

The fan has eight forward swept blades and a diameter of 370 mm, the entire shroud has a area of 470*670 mm^2 and is equipped with three flaps to let the air bypass the fan at high ram air flows. It has a control module for connection of the power supply and signal wires needed to drive the fan and four struts to support the motor, shown in Figure 3.3.

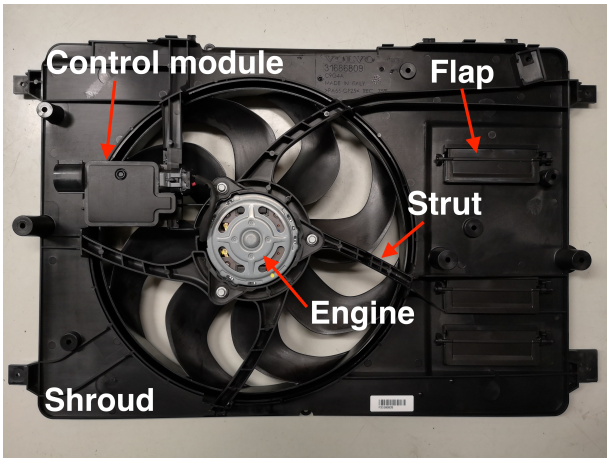

Figure 3.3: *Rear of the fan with the control module, flaps, struts, engine and shroud highlighted*

The fan was rigidly mounted with a steel construction containing two square beams with plates on both ends that could be fastened in the ceiling and floor of the wind tunnel. On the two vertical beams the fan shroud could then be attached with screws. The fan mounting is shown in Figure 3.4. In order to reduce the influence of the walls on the flow field the construction was centered in the tunnel with respect to the fan rotational axis and not to the shroud , therefore the distance between one wall and the shroud was smaller than on the opposite side. The shroud attachments to the beams were placed on the short sides, as far from the rotating fan part as possible, to minimize the flow disturbance of these two in the region downstream of the fan.

Figure 3.4: *Fan mounting in the wind tunnel*

To run the fan, a DC power supply was used where the required voltage could be set and the rotation speed was regulated with a PWM-controller. Pulse width modulation, PWM, is a simple and effective way of controlling the speed of DC motors. PWM uses a digital source to create a square wave that switches the voltage on and off much faster than the controlled device can discern. By defining the frequency and cycle width of the signal the amount of power applied to the motor can be controlled [15, 16]. To measure the fan rotation speed, an optical tachometer was used that measures the revolutions per minute with a laser directed at a reflective tape put on the fan. By optical access through the transparent walls the rotation speed could be measured from outside the tunnel, which was necessary since the wind tunnel flow will influence the fan rotation speed.

Just as for the initial verification measurements the laser probe was mounted on a cylinder connected to the traverse for an easy movement of measurement position in the y- and z-direction. To obtain the streamwise and vertical cross-stream velocity components the probe was mounted horizontally normal to the flow, as in Figure 3.5, and rotated 90 degrees to a vertical position normal to the flow to get the third velocity component in cross stream direction.

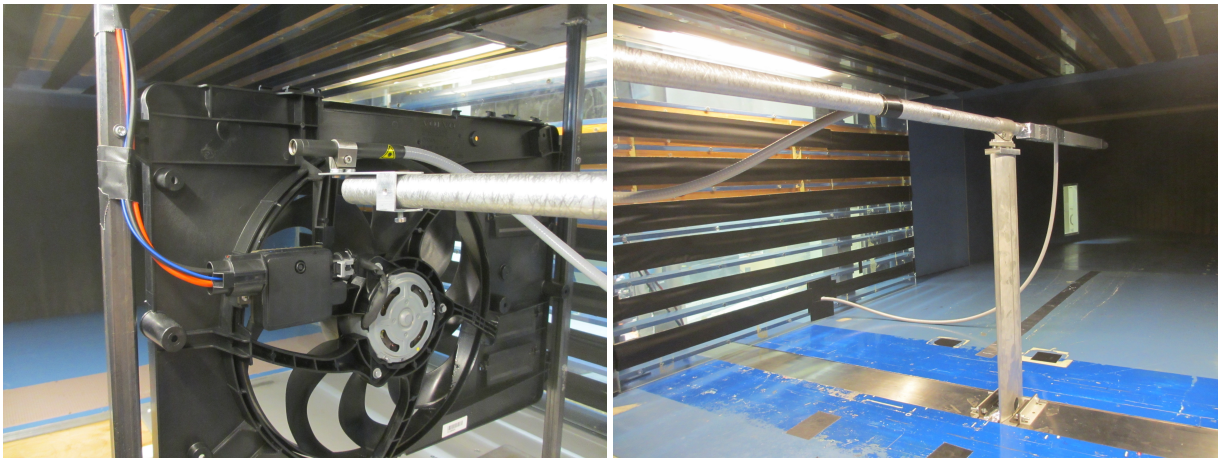

Figure 3.5: *Horizontal probe mounting on cylinder (left) and cylinder mounting on traverse (right)*

For all tests performed the slotted walls in the wind tunnel were covered with tape to avoid the possible influence of the slotted walls on the wake. Further, the CFD simulations used for comparison were performed with solid walls.

3.2.2 Data Acquisition

In the BSA flow software the number of particles collected at each position was set to 10000 in x-direction and 5000 in z-direction or a maximum of 10 seconds. The data rate (validated burst rates) varied much depending on the probe position but at an average of around 1000 Hz in x-direction and 500 Hz in z-direction. Again, transit time weighting was applied to the data to remove velocity bias effects. The choice of software settings was based on guidelines from the BSA Flow Software User Guide [17] but optimized for the specific set-up and measurements in this study.

Since the LDA system measures the velocity of every particle passing through the measurement volume, the obtained velocities at each position will not all be the same. In the software one must define in what velocity range particles will be measured in, to eliminate single particles that would distort the measurements. It is preferred to set a large velocity span initially that during test can be modified to not disregard any particles passing the measurement volume and to obtain a correct average. To set the centre and span of obtainable velocities, test measurements was initially performed at a few different positions where large magnitude velocities were expected to define a suitable velocity range.

The sensitivity and gain of the signal was for the majority of the tests set to 1000 V and 20 dB in x-direction and 1200 V and 22 dB in z-direction. The sensitivity sets the highest level of voltage to the photo-multiplier and gain sets the power increase of the signal.

Figure 3.6 shows how a histogram of velocities at a position can look during a measurement where the count of measured particles in percent is plotted over velocity. The red curve is a normal, or Gaussian, distribution adjusted to the shape of obtained velocities.

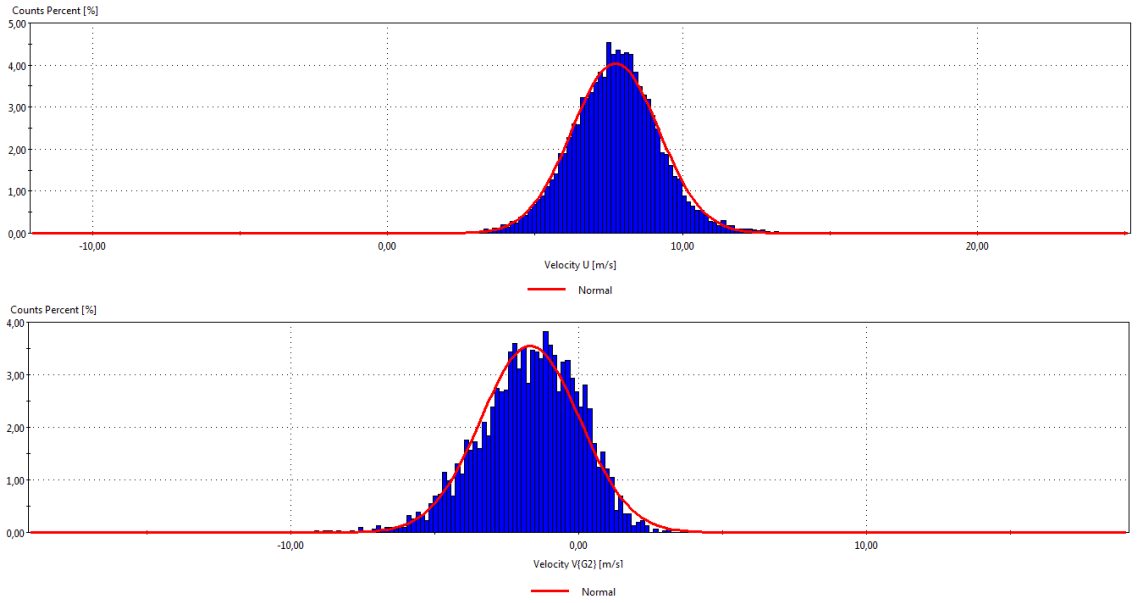

Figure 3.6: *Histogram of measured velocities in streamwise direction (top) and in vertical cross-stream direction (bottom)*

In Figure 3.7 the system monitor can be seen, which is where the measured Doppler bursts are showed and works as a tool to optimize the processor settings. The yellow vertical lines are the record length sent to the processor to determine the frequency. An *Auto adaptive mode* was used that automatically sets the record length for each individual burst, between the yellow lines. The two inner lines indicates the number of samples collected for the maximum record length and the outer lines sets number of samples for the shortest records length. The record length should ideally match the shortest bursts of the measured signal but the processor is robust to change from the ideal signal.

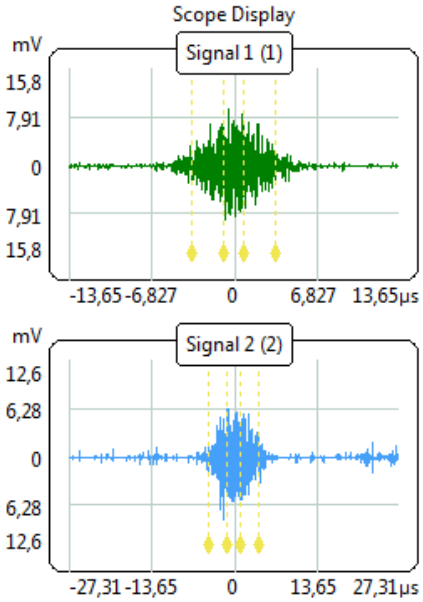

Figure 3.7: *System monitor showing the burst signals in streamwise direction (top) and in vertical cross-stream direction (bottom)*

3.2.3 Measurements

Tests were preformed with several different configurations at different planes downstream of the fan. Two different fan rotations speed was tested, 1400 rpm and 2800 rpm, which corresponds to typical operation speeds in a vehicle. First the streamwise (x-direction) and vertical cross-stream velocity component (z-direction) were studied at planes 4, 8 and 12 cm downstream the fan. Then the horizontal cross-stream velocity component (y-direction) was measured by changing the probe setup to get a full three-dimensional study of the flow characteristics. The coordinate system is shown in Figure 3.8

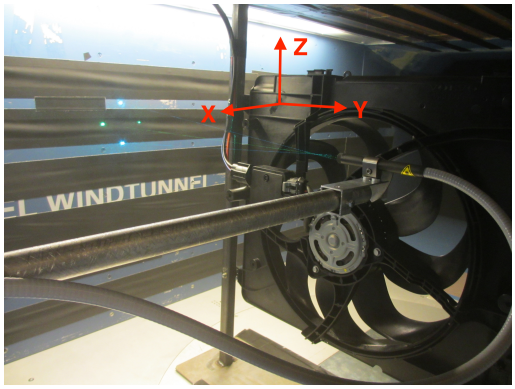

Figure 3.8: *Coordinate system*

To reduce the measurement time, the measurements were focused on the region behind the fan and not the entire shroud. The measured region can be seen in Figure 3.9. Since several configurations were studied at the different planes a quite coarse mesh was used for these measurements. For the initial tests the measured area were 400*400 mm^2 but the width was expanded 20 mm on the left side to even out the measured distance on both sides of the fan, so the measured area were 420*400 mm^2 for the majority of the tests. The step size between each measurement point were 20 mm in both y- and z-direction, giving a total of 462 points. With the overall fan flow behaviour determined, the interesting flow regions could later be investigated further with a finer mesh. The reason for why the measured distance, with respect to the fan centre, in vertical direction is smaller on the upper side compared to the lower is that the traverse were not able to reach higher.

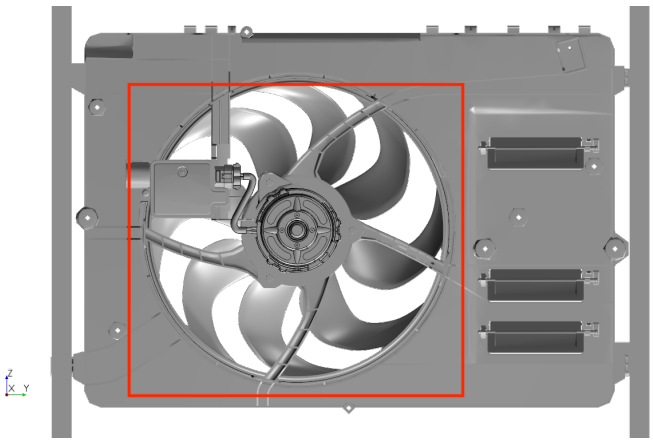

Figure 3.9: *Measured area with coarse mesh*

For the two-dimensional coarse mesh study a total of eight different configurations was measured at the three different planes downstream. To analyze the flow field at idle running, the fan was tested for rotations speed of 1400 and 2800 rpm with no wind tunnel speed. Then with only wind tunnel speed of 5 and 10 m/s to study how the fan and the flow behaves only driven by the natural inflow of air. Finally combinations of fan rotation and wind tunnel speed for both 1400 and 2800 rpm with 5 and 10 m/s wind tunnel flow respectively were tested. The different test cases can be seen in Table 3.1. Since the wind tunnel flow also contributes to the fan rotation speed, for the later four configurations, the correct rotations per minute was set with the power supply with the wind tunnel running.

Table 3.1: Test cases

Test	Fan rotation speed [rpm]	Wind tunnel velocity [m/s]
1	1400	0
2	2800	0
3	0	5
4	0	10
5	1400	5
6	1400	10
7	2800	5
8	2800	10

First the traverse was calibrated so that the position settings in the BSA software corresponds to a correct length movement of the traverse. This was made with a trial and error study by setting distance in the software and measure the actual movement of the traverse.

The freestream velocity of the wind tunnel was measured at test section without the fan mounted. The wind tunnel setting to get the investigated velocities was noted so that the same velocities can be used for the different configurations. The turbulence intensity of the wind tunnel was also measured with the LDA system in the centre of the wind tunnel for the freestream velocities. The turbulence intensity at the probe position 4 cm downstream is 0.54 % for a freestream velocity of 5 m/s and 0.49 % for 10 m/s. At the location 12cm downstream the turbulence intensity is 0.45 % for a velocity of 5 m/s and 0.43 % for 10 m/s.

All measurements with wind tunnel running were performed with boundary layer suction. Due to the absence of boundary layer without wind tunnel flow, no boundary layer suction was used for the cases with only a fan forced rotation in order to not disturb the local flow around the fan. The fan rotation speed was measured, from outside the wind tunnels transparent window, multiple times during each test to make sure that the rotation speed was kept constant.

From the verification measurements it was clear that the seeding is a very important parameter for the measurements. In order to keep an even seeding density smoke was generated at different rates depending on the configuration tested, but in general a two second burst of smoke every 20 seconds provided a good seeding with the 400 W smoke machine used in this study.

To make sure that sufficient seeding was generated the count and data rate in the

software was constantly monitored since these two parameters heavily depend on the seeding density and should to be kept at sufficiently high levels. Also, the laser beams was checked during measurements as their degree of visibility seemingly rely upon the amount of seeding particles in the air. In Figure 3.10 one can see the laser beams due to the presence of smoke in the tunnel.

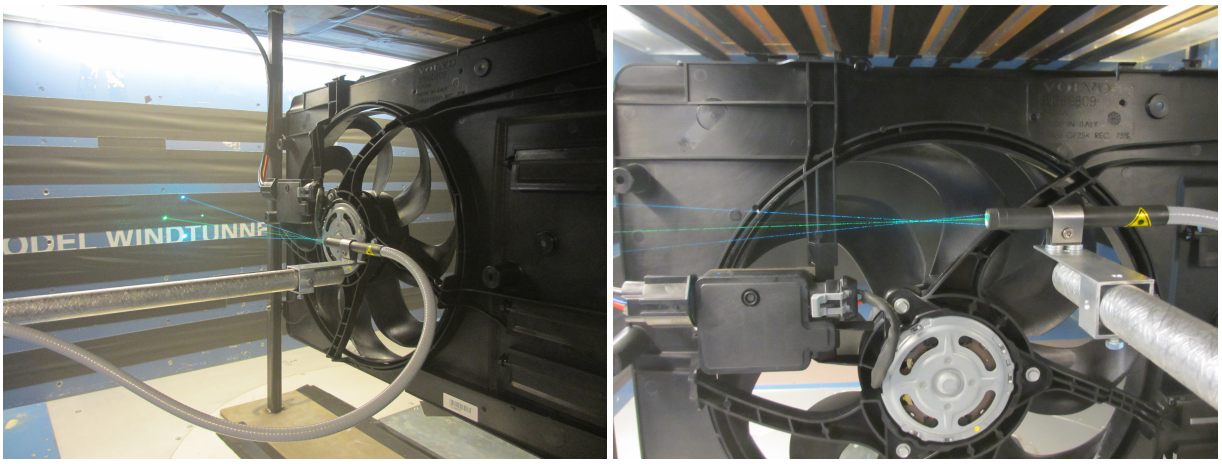

Figure 3.10: *LDA measurement in the fan wake*

Just as for the cylinder measurements, the smoke machine was located downstream of the cylinder for all tests with wind tunnel air flow. It was placed in the blocked passage behind the slotted walls and did therefore not disturb the flow. For the measurements without wind tunnel flow the smoke machine was instead placed upstream of the fan to get the flow to pass through the measured region. Obviously this will not generate an as even seeding density as for the downstream smoke machine placement with the wind tunnel running, but was considered the best achievable way for these cases.

Since the largest flow variations took place behind the control module and fan supporting struts these regions were investigated further with finer measurement meshes. The flow downstream of the control module was studied with a mesh containing 520 measurement points and a step size of 10 mm over a 190*250 mm^2 area, shown in Figure 3.11 (1). The measured region for the right strut was 140*100 mm^2 with a step size of 5 mm giving 609 points, visualized in Figure 3.12 (2). Both regions were measured for 1400 and 2800 rpm with a wind tunnel speed of 5 m/s in the plane 4cm downstream. For the case with a wind speed of 5m/s and a fan rotation of 1400 rpm, also the lower strut was measured with 238 points and a step size of 10 mm distributed over a region of 130*160 mm^2, shown in Figure 3.12 (3).

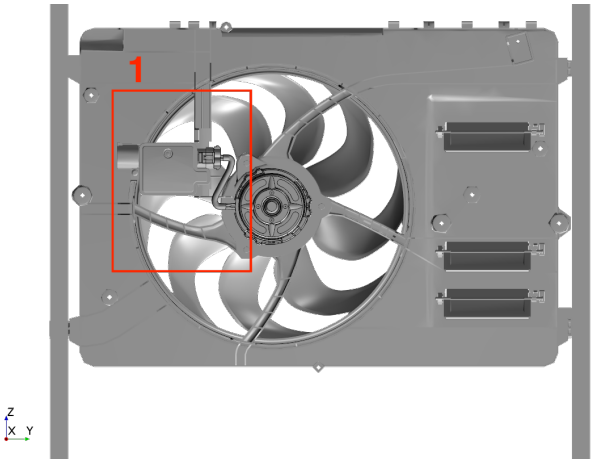

Figure 3.11: *Measured area control module*

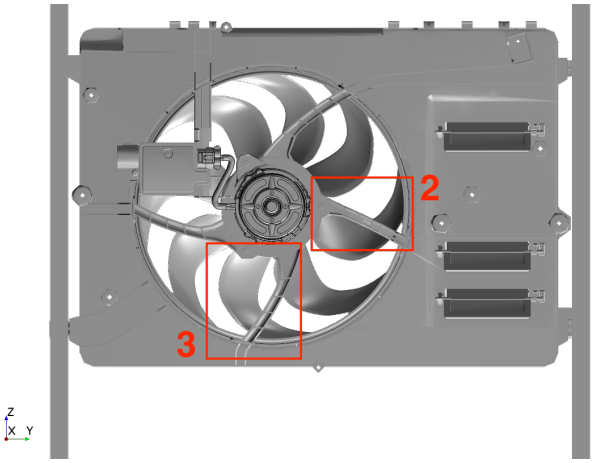

Figure 3.12: *Measured areas struts*

Finally, the upper half of the fan was measured with the probe mounted vertically in order to obtain the third velocity component in y-direction. The reason for why only the upper half of the fan was measured was because the probe cable could not be lowered more than that before hitting the floor. But instead this set-up gave the opportunity to measure a higher region above the fan, so the starting point was set 40 mm higher. The measured area was 420*290 mm^2 with a step size of 20 mm and can be seen in Figure 3.13 (4). When desired to obtain the velocity components in all three directions with a 2D probe it is important to set the same start measurement point after redirecting the probe. With the vertical position of the probe the velocity components in the horizontal cross-stream direction and streamwise direction was measured.

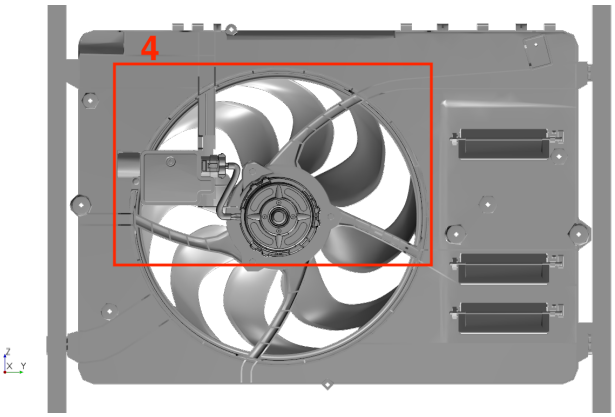

Figure 3.13: *Measured area upper half*

3.2.4 Data Processing

For the processing of the results Matlab was used. The amount of measured points was only enough to give a coarse representation of the velocity field. Therefore, to clearly visualize what the flow looks like, a cubic interpolation was done. A linear interpolation was also tested but the cubic interpolation gave a smoother velocity field visualization more similar to the corresponding CFD simulation, presented in section 4.2.2. The comparison can be seen in Figure 3.14 where the velocity field from a linear interpolation between the measurement points is compared with a cubic interpolation for the case with a wind tunnel speed of 5 m/s and a forced fan rotation of 2800 rpm. Similarly as for the cylinder study, fast Fourier transform was used for the spectral study of the fluctuating velocities.

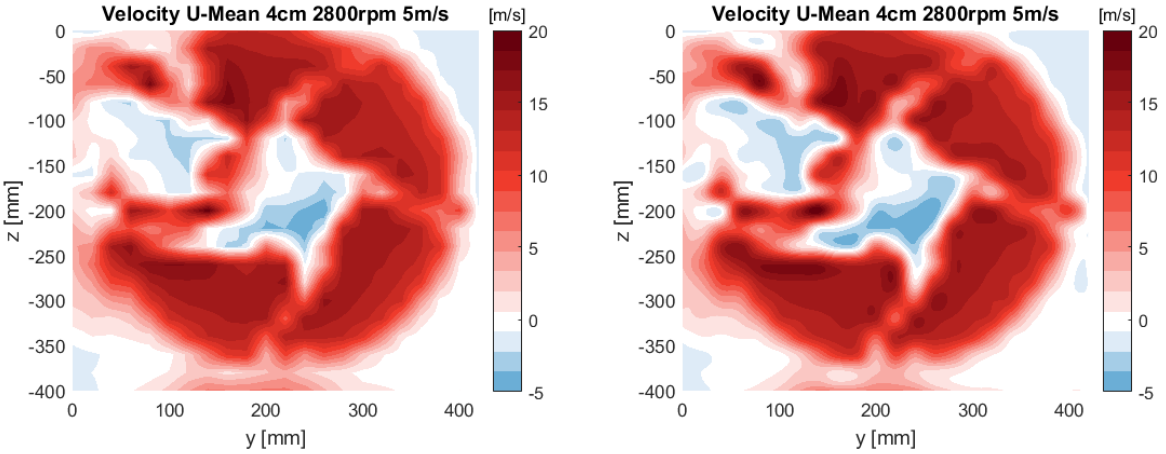

Figure 3.14: *Comparison of linear interpolation (left) and cubic interpolation (right)*

4 Results and Discussion

In this section the results of the cylinder and fan measurements are presented and discussed. Finally the uncertainties of the measurements are explained.

4.1 Cylinder Wake Measurements

For comparison, similar LDA studies of cylinder wake flow made by C. Norberg [13, 14] are used. These studies are suitable to use for comparison, since they present the results normalized by characteristic data, such as the freestream velocity and the cylinder diameter. Norberg presented plots of the mean streamwise velocity as a function of downstream distance along the wake centerline.

In the present study, at wake centerline four diameters downstream of the cylinder the normalized mean streamwise velocity is 0.718 when scaled with the freestream velocity of 4.82 m/s (Re=8000). The streamwise velocity is an average based on two measurements. This value can be compared to the scaled velocity of around 0.73 that Norberg obtained at a downstream distance of four diameters for the same Reynolds number. The corresponding value for the streamwise RMS velocity, in this study, is 0.186 compared to approximately 0.18 from Norberg's measurements. The comparisons show a good agreement, the streamwise velocity measured in this study is about 1.6 % lower than the value obtained by Norberg while the measured streamwise RMS velocity is approximately 3.2 % higher compared to Norberg's value.

The measured streamwise velocity at two diameters downstream is 0.23 compared to Norberg's 0.32 and the RMS velocity 0.29 compared to 0.32. Which shows an increased variation compared to at four diameters downstream. The larger deviation could be due to the higher turbulence intensity in this study that causes the wake to recover faster and therefore gives different values.

The wake centerline measurement at one diameter downstream give poor results due to that at several positions across the wake very few particles are captured. The reason for this is likely a combination of a uneven seeding density and the difficulty to capture particles in the near cylinder wake following the cylinder blockage. From this comparison it is clear that the closer to the cylinder the measurements are performed, the less accurate results are obtained.

Figure 4.1 shows a measurement of the mean streamwise velocity across the wake. The y-axis for the velocity is scaled with the freestream velocity and the distance on the x-axis scaled with the cylinder diameter. The measurements is performed from the wake centerline (y=0) and outwards across the wake in one direction. From the comparison with Norbergs plots, shown in Figure 4.2, the curves shows similar characteristics, especially for the x/D=1 case. For the x/D=2 case near the wake centerline one can see that Norberg obtained values of approximately 0.3 while is this study was about -0.2. The difference is most likely due to the differences in set-up and wind tunnel conditions. Note that the line marked with triangles, for a Reynolds number of 8000, is the one compared to.

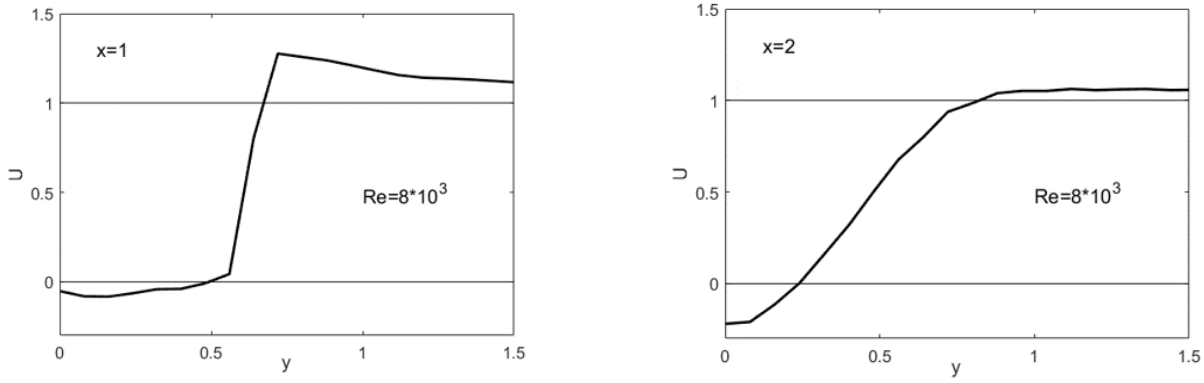

Figure 4.1: *Mean streamwise velocity measurements across the wake for a Reynolds number of 8000 at one diameter downstream (left) and two diameters downstream (right)*

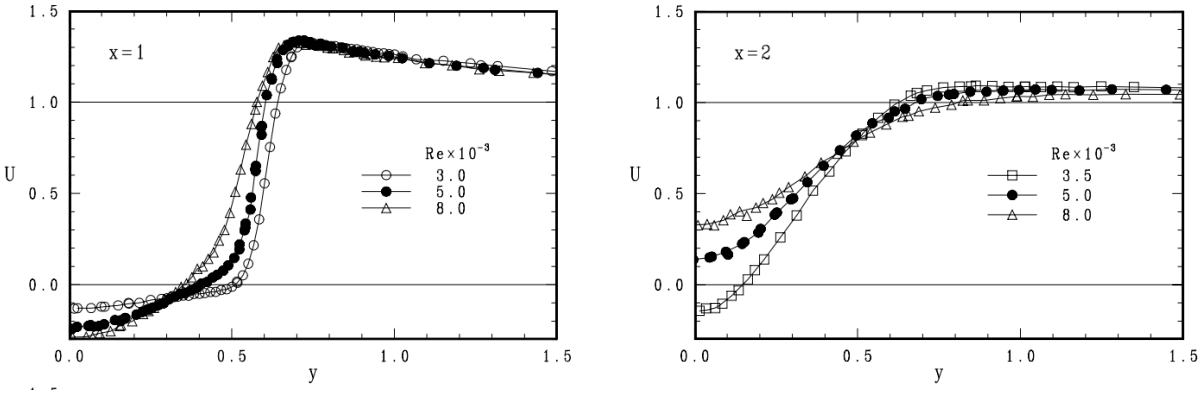

Figure 4.2: *Mean streamwise velocity from Norbergs measurements across the wake for a Reynolds number of 8000 at one diameter downstream (left) and two diameters downstream (right), source [13]*

At some positions, along the wake centerline, a dominant vortex shedding frequency could not be detected, but a bit off the centerline a clear peak occurred close to the one reported in literature of 0.2 [14]. This can be seen in Figure 4.3 where the frequency spectrum at centerline is compared with the spectrum at 8 mm away from the centerline in y-direction.

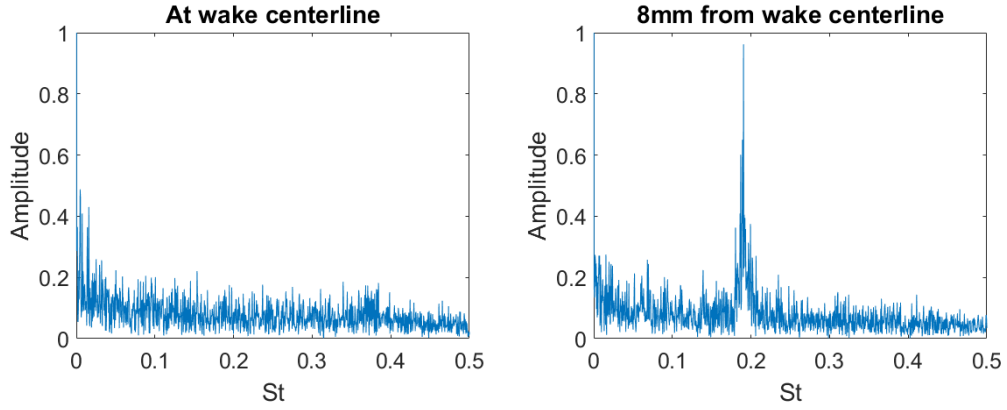

Figure 4.3: *Comparison of frequency spectrum for x/D=4, Re=20000*

The reason for this can be that the turning vortices in the wake does not cross the wake centerline, as illustrated in Figure 4.4.

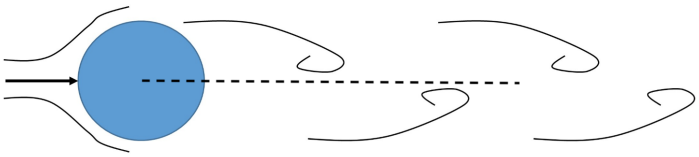

Figure 4.4: *Turbulent wake downstream a circular cylinder*

Table 4.1 shows a Strouhal number comparison at different Reynolds numbers and downstream distances. It should be noted that the Strouhal number is normally determined at the wake centerline but the values from this test are based on an average of values across the wake. The measurements are performed from the wake centerline and 10 mm in both positive and negative y-direction with a step size of 2 mm, giving a total of 11 values. Some of the calculated average Strouhal numbers are based on fewer values since, as mentioned, at some measurement positions near the wake centerline, it is not possible to distinguish a clear peak in the frequency spectrum.

Table 4.1: Strouhal number comparison for different Reynolds number

Re	St, x/D=2	St, x/D=4	$St_{C.N}$	Δ, x/D=2 [%]	Δ, x/D=4 [%]
8000	0.2147	0.2031	0.203	17.79	0.7847
15000	0.2027	0.1897 (0.1900)	0.195	6.966	2.448
20000	0.2011	0.1895 (0.1899)	0.191	8.516	2.509
30000	0.2015	0.1851 (0.1855)	0.189	6.613	3.928

For the measurements at four diameters downstream for Reynolds numbers of 15000, 20000 and 30000 there is a single Strouhal number value that deviated from the trend of the other measured values across the wake. The values showed in parenthesis is the average of the measured Strouhal numbers neglecting the deviating value. Since the deviating value is most likely due to a measurement error, this will show a more valid Strouhal number. The Δ-values shows the range of the measured Strouhal numbers, i.e. the relative difference between the lowest and highest values obtained. It should be mentioned that the values compared with, $St_{C.N}$ are estimates from Norbergs Strouhal over Reynolds number graph Figure 4.5.

As can be seen the Strouhal numbers measured along the wake centerline at four diameters downstream of the cylinder agrees quite well with the corresponding values from Norbergs study. This is visualized in Figure 4.5 which shows a plot of Strouhal number over Reynolds number from Norbergs measurement in the wake region $x/D < 5$ [14]. The red dots illustrate the Strouhal numbers measured in this study at four diameters downstream of the cylinder. The values at two diameters downstream of the cylinder give less accurate results leading to an overestimated Strouhal number.

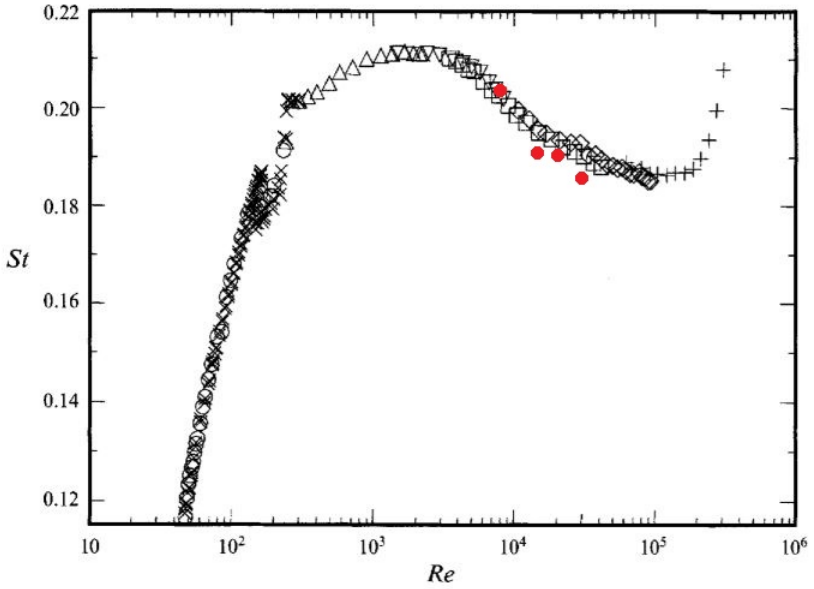

Figure 4.5: *Strouhal over Reynolds number plot used for comparison of the Strouhal numbers measured in this study (red), source [14]*

Figure 4.6 illustrates the frequency spectrum at four diameters downstream for a Reynolds number of 8000. At a position of 2 mm from the wake centerline in both positive and negative y-direction another peak could be detected in the spectrum located at around 0.4. The amplitude of this peak is not as strong as the one at a Strouhal number of 0.2 but it occurs at an exactly double frequency, indicating a symmetrical vortex shedding at these specific locations.

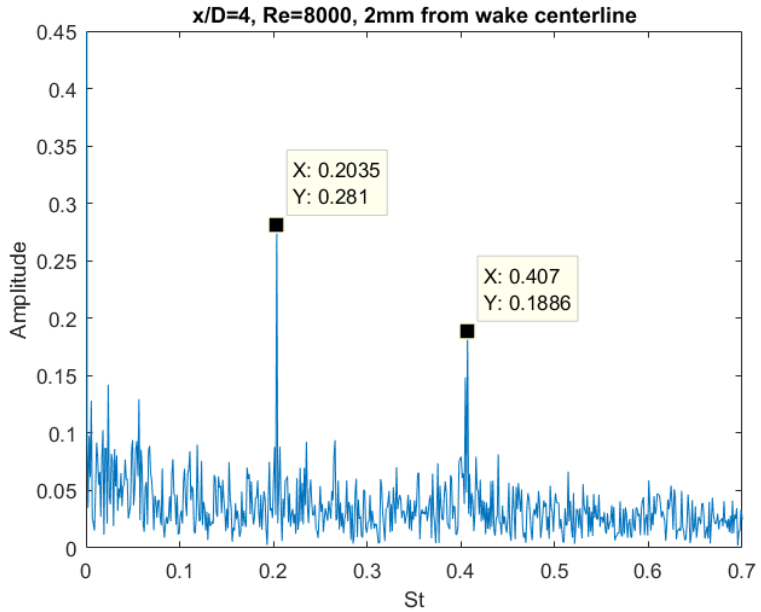

Figure 4.6: *Symmetric frequency shedding visualized in the frequency spectrum for 2 mm from the wake centerline*

Error sources could be the cylinder vibrating, even though no visible vibrations could be noted at the measured velocities. Also vibrations of the probe could cause noise disturbing the frequency shedding and making it hard to distinguish peaks in the spectrum. These errors could be confirmed as with increasing Reynolds number, more fluctuating values could be detected with an overall higher amplitude in the frequency spectrum. Looking at the sixth column in Table 4.1 one can see that the at four diameters downstream the range of measured Strouhal numbers increases with increasing Reynolds number. The reason for this is believed to be the higher oscillations of the cylinder and probe at higher freestream velocities.

For two diameters downstream of the cylinder, the range between the highest and lowest measured Strouhal numbers seems to be the opposite, compared to at four diameters downstream. Here the largest range occurs for the low Reynolds numbers instead, shown in the fifth column in Table 4.1. At this downstream distance, the variation of measured Strouhal numbers across the wake is also overall much higher compared to four diameters downstream. This further indicates that it is harder to obtain accurate measurements closer to the cylinder.

It showed, that keeping a constant seeding density by controlling the smoke machine manually, was one of the highest difficulties. This is most likely the main source of measurement errors. A timer that automatically provides new seeding particles, could improve the set-up.

It should be noted that Norbergs measurements were performed in a smaller wind tunnel with a different blockage ratio and turbulent intensity. Also, Norberg used a solid 6 mm steel cylinder with different aspect ratio compared to the hollow one used in this study. But since the cylinder and plate used in this study also is made of steel it is still a rigid construction. Norberg had the cylinder mounted at both ends while in this test the cylinder is only mounted rigidly at the top, however no notable vibrations of the cylinder can be observed for freestream velocities up to the maximum velocity of 18 m/s.

In comparison with other studies [13, 14], having in mind that the the wind tunnel conditions and cylinder setup were not identical, the behaviour of the wake in terms of vortex shedding (St-number) agrees well. For the normalized velocities, exactly matching values were not obtained but the characteristics of the curves were similar. The measurement equipment and execution procedure can therefore be considered accurate, generating physical results.

4.2 Fan Measurements

In this section the results of the fan measurements is presented and discussed. Starting with the investigation of the entire fan induced flow field at the three planes, a spectral analysis of velocity fluctuations and lastly the measurement uncertainties. All the velocity plots shown below are at planes downstream of the fan seen from behind, so the rotational direction is counterclockwise.

4.2.1 4 cm Downstream

This section presents plots of the velocity field in a plane 4 cm downstream of the fan.

Streamwise

In Figure 4.7 and 4.8 the streamwise velocity component for wind tunnel speeds of 5 and 10 m/s, without forced fan rotation, is plotted in the yz-plane 4 cm downstream of the fan. The blockage by the fan motor, in the centre, and the control module, in the upper left corner, causes low velocities in these regions. A similar flow behaviour with reduced velocities is observed downstream the shroud surrounding the fan. The freestream wind tunnel velocity of 5 m/s causes a fan rotation that contributes to increasing the velocity of the wind to a maximum velocity of about 5.2 m/s. The highest velocities seem to occur along the blade span close to the blade tip and decreases towards the hub, which make sense because of the higher circumferential speed.

When increasing the wind velocity to 10 m/s, one can see that the higher velocities are distributed over the entire blade span but still with increasing magnitude towards the tip. This is due to that the wind tunnel velocity of 5 m/s only causes a fan rotation speed of about 200 rpm while the 10 m/s case gives a rotation speed of over 1200 rpm. The position of the four struts supporting the fan motor can now be distinguished more clearly as their blockage of the high speed flow cause decreased downstream velocities. It appears that the highest velocities occur around the control module. The reason for this is the acceleration of the flow passing through these confined spaces. The blue regions downstream the blocked areas indicate slightly reversed flow.

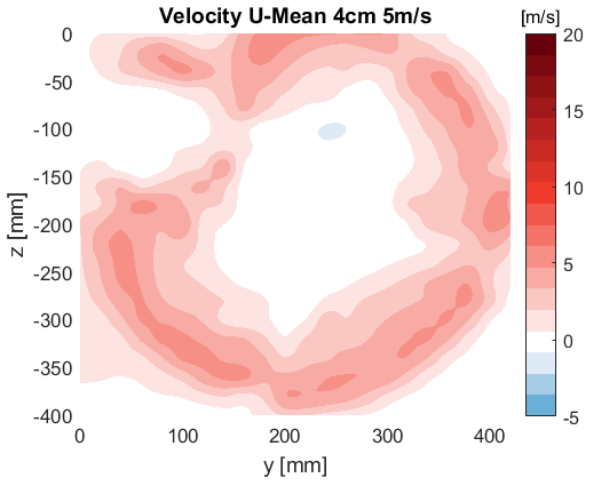

Figure 4.7: *Streamwise velocity 5 m/s wind*

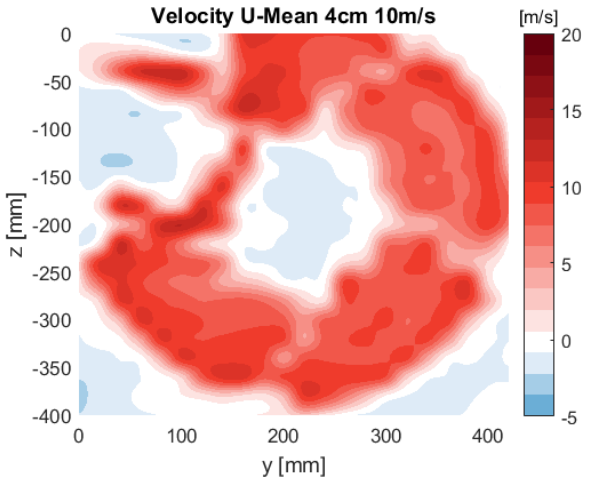

Figure 4.8: *Streamwise velocity 10 m/s wind*

Figure 4.9 and 4.10 shows the streamwise velocity component for a test with a fan rotation speed of 1400 and 2800 rpm respectively, without wind tunnel flow.

The higher rotation speed of 2800 rpm gives a streamwise flow field with high velocities in the regions without blockage. Over the blade span the velocities are now highest near the hub and decreases towards the tip. The reason for this is believed to be due to geometrical differences. In the centre of the fan where the engine is placed the fan have a larger depth compared to at the tip region and therefore the flow accelerates around this larger area.

This case shows streamwise velocities around 0 m/s downstream of the shroud in comparison to the case with only wind speed where the wind tunnel flow is contributing to a slightly reversed streamwise flow. On the contrary, for the case with only power supplied to the fan, the flow downstream the motor shows a stronger tendency of reversed flow.

Due to the absence of circulating flow in the tunnel for these cases, the smoke machine is placed upstream of the fan, generating smoke only in the test section that is sucked through the fan as it is rotating. For the test with wind tunnel flow the smoke machine can as mentioned be placed downstream of the object and generate smoke circulating through the whole tunnel, giving a complete filling with an even density. By studying the visibility of the laser beams, indicating that there are sufficient particles in the tunnel, the upstream placement of the smoke machine seemed to be working rather well, but is not the optimal way of seeding. Thus, the tests are still included since they results in a good overall visualization of the flow behaviour only caused by the fan.

Note that the results from the case with a fan rotation of 1400 rpm, shown in Figure 4.9 is not fully accurate since it is the first test performed on the fan and the software settings adjusted during the measurement. This can be seen on the upper part where the flow shows a strange behaviour and the sudden drop in velocity at a point in the lower left region is most likely due to an measurement error.

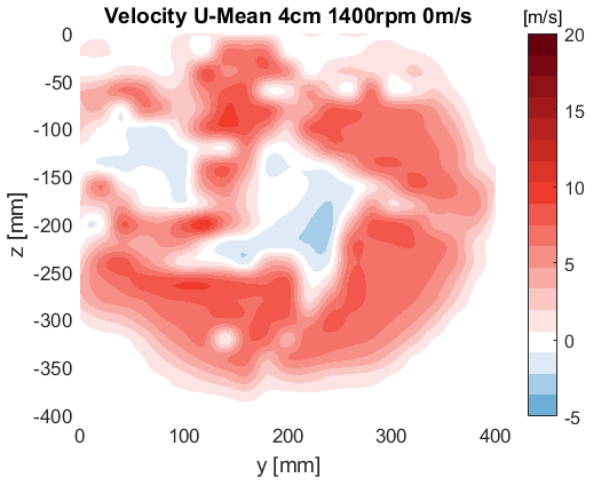

Figure 4.9: *Streamwise velocity fan rotation 1400 rpm*

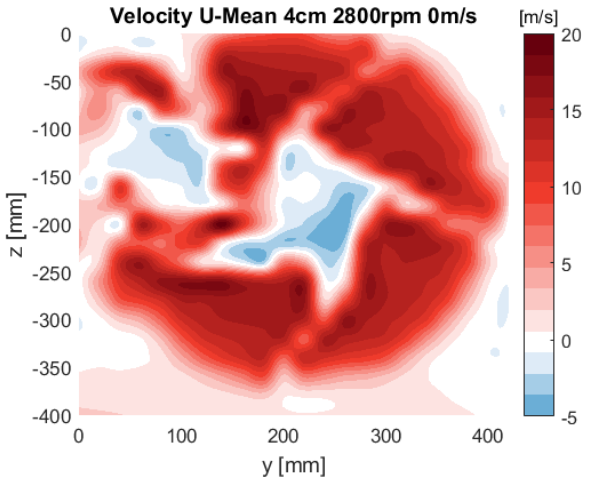

Figure 4.10: *Streamwise velocity fan rotation 2800 rpm*

A combination of both wind tunnel flow of 5 m/s and fan rotation speed of 1400 and 2800 rpm is shown in Figure 4.11 and 4.12. For both cases the low speed of the wind tunnel has a moderate effect on the streamwise velocity component compared to cases without the tunnel air flow. Just as for the previous cases the highest velocities occur

around the control module. Now, with the presence of wind flow, the regions downstream the shroud are again characterized by areas of reversed velocities as seen in the top right and bottom left corners of the measured area.

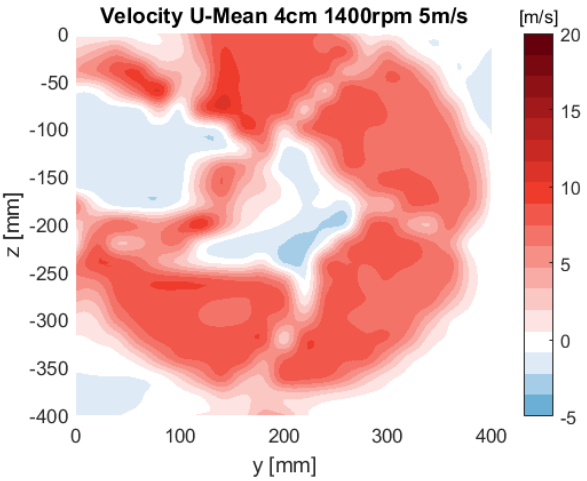

Figure 4.11: *Streamwise velocity fan rotation 1400 rpm and wind 5 m/s*

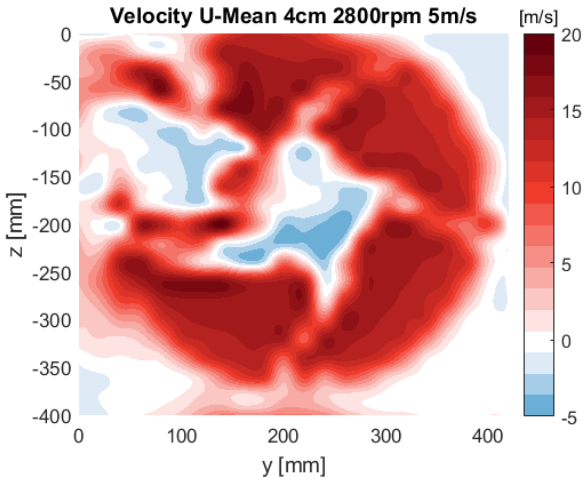

Figure 4.12: *Streamwise velocity fan rotation 2800 rpm and wind 5 m/s*

When increasing the velocity of the wind tunnel air flow to 10 m/s while keeping the fan rotation speed to 1400 and 2800 rpm, respectively, there is an overall increase of velocities compared to the 5 m/s case, illustrated in Figure 4.13 and 4.14. The maximum velocities again occur around the control module. For both rotation speeds the measured area with high velocities in the top left corner, confined by the control module and its supporting beam, is growing as the wind tunnel speed increases.

Again, note that the rotation speed is set with both the wind tunnel and power supply contribution. Meaning that with increasing wind tunnel velocity, less power was supplied to the fan in order to maintain the investigated rotation speeds.

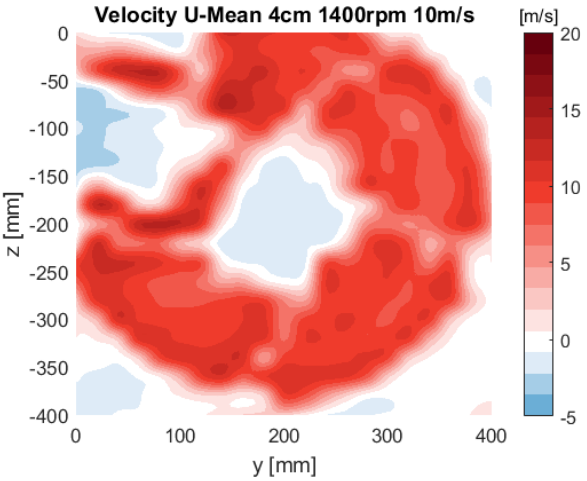

Figure 4.13: *Streamwise velocity fan rotation 1400 rpm and wind 10 m/s*

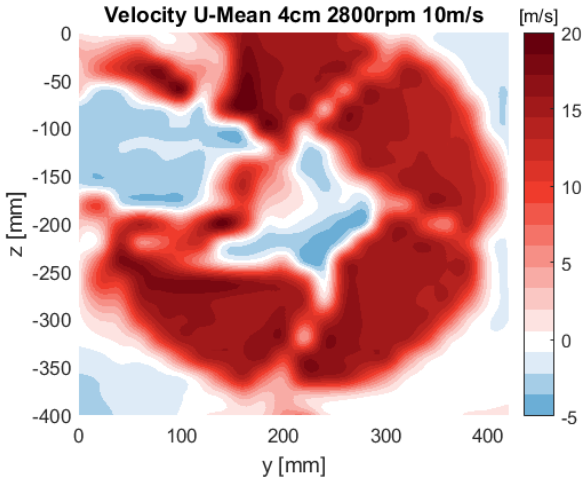

Figure 4.14: *Streamwise velocity fan rotation 2800 rpm and wind 10 m/s*

Vertical Cross-Stream Component

When looking at the vertical cross-stream velocities, shown in Figure 4.15 and 4.16, one can see that the upper half is characterized by positive velocities and the lower half dominated by negative velocities, but of the same order of magnitude. (Directly downstream the fan it should be a horizontally directed flow at the upper and lower half due to the fan rotation. But, since the measured plane is further downstream the flow has turned by about 90 degrees, and therefore appears divided between the top and bottom.) So, the air being sucked through the fan spreads outwards at the fan exit, following the centrifugal force, to reunite with the wind tunnel flow. This outward turning effect is not as strong on the sides, as for the upper and lower regions, since there are more blockage by the shroud and mounting beams in these directions.

For the wind tunnel speed of 10 m/s a similar behaviour as for the 5 m/s case can be seen, but the regions with highest positive and negative velocities seems to be rotated slightly in clockwise direction, illustrated with the grey dividing lines. As the increased wind velocity, without forced fan rotation, causes the fan to rotate faster it will have a bigger impact on the flow compared to the 5 m/s case where the flow passing through the fan is less influenced by the slower rotation.

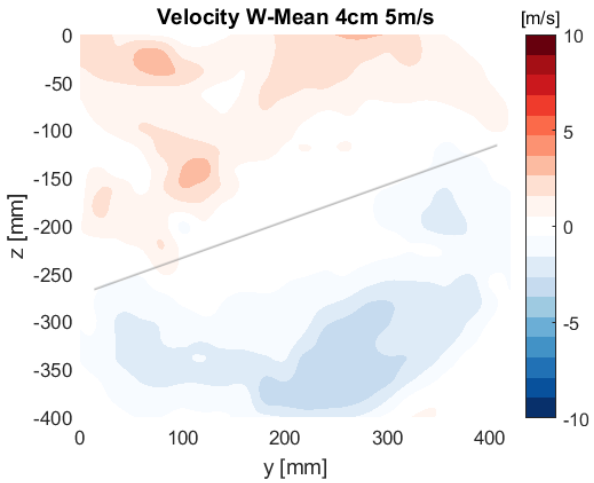

Figure 4.15: *Vertical cross-stream velocity wind 5 m/s*

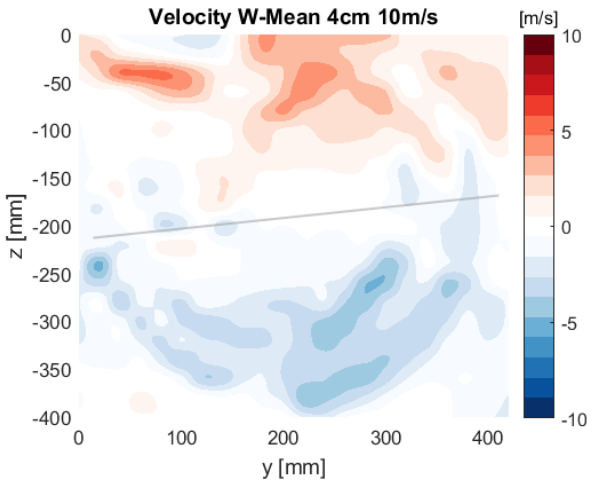

Figure 4.16: *Vertical cross-stream velocity wind 10 m/s*

Figure 4.17 and 4.18 illustrates the vertical cross-stream velocities with no wind tunnel flow for 1400 and 2800 rpm respectively. In comparison to the tests with only wind tunnel speed the cross-stream velocity behaviour is very different. The regions with positive and negative velocities are now, compared to the cases with only wind tunnel flow, rotated 90 degrees clockwise and mainly divided between left and right half.

The reason for this is that the measurement in this direction only captures high velocities on the sides where the fan rotation forces the flow upwards on the right side and downwards on the left side. At the top left region the blockage of the control module instead forces the flow up. Since no wind velocity will affect the upper and lower regions these areas will be dominated by flow moving horizontally with low vertical directed velocities.

Note that the scale differs between the compared plots of the horizontal cross-stream velocity to increase the visibility of the flow behaviour for the lower fan rotation speed.

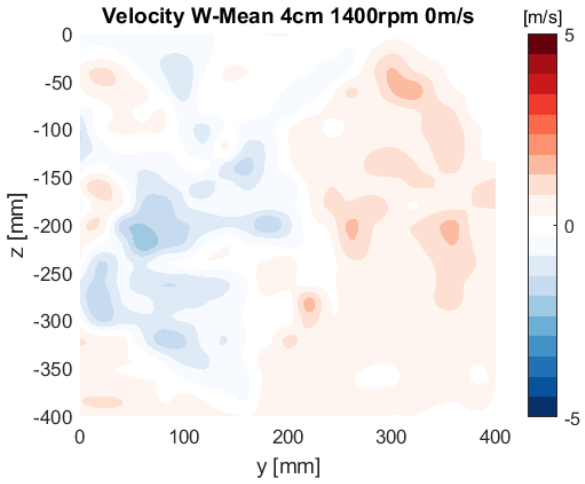

Figure 4.17: *Vertical cross-stream velocity fan rotation 1400 rpm*

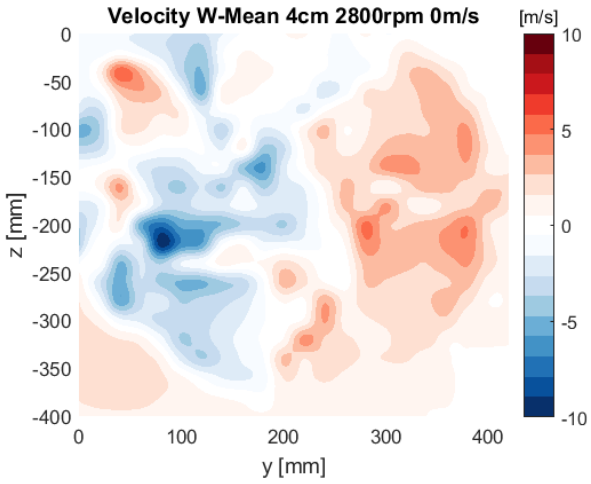

Figure 4.18: *Vertical cross-stream velocity fan rotation 2800 rpm*

Introducing a wind tunnel speed of 5 m/s results in a very similar velocity field for both fan rotation speeds, illustrated in Figure 4.19 and 4.20. The biggest variation in comparison to the case without wind tunnel flow are the larger velocities in the region above the control module.

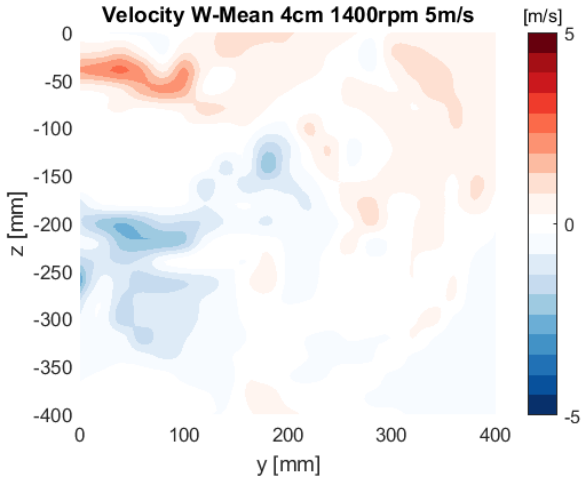

Figure 4.19: *Vertical cross-stream velocity fan rotation 1400 rpm, wind 5 m/s*

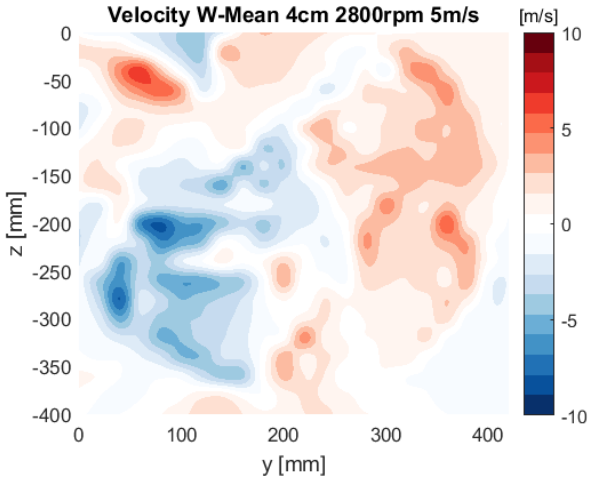

Figure 4.20: *Vertical cross-stream velocity fan rotation 2800 rpm, wind 5 m/s*

By increasing the wind tunnel speed to 10 m/s, the velocities for the case with a rotation speed of 1400 rpm show a similar behaviour as for the case with only wind tunnel flow. With velocities directed upwards on the upper half and downwards at the lower half, as can be seen in Figure 4.21. This is due to that the stronger wind flow will have a high impact the flow field at this low rotation speed. For the case with 2800 rpm, shown in Figure 4.22, the higher fan rotation speed causes a flow field less influenced by the wind tunnel flow compared to the 5 m/s case.

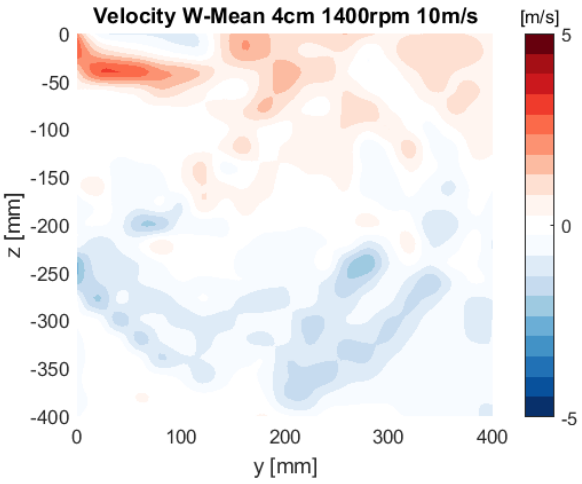

Figure 4.21: *Vertical cross-stream velocity fan rotation 1400 rpm, wind 10 m/s*

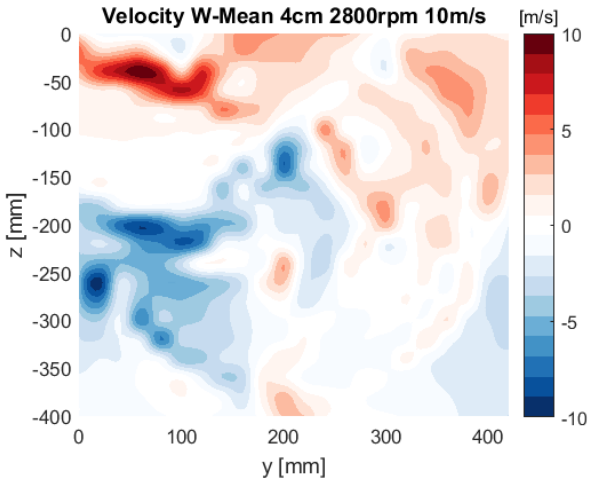

Figure 4.22: *Vertical cross-stream velocity fan rotation 2800 rpm, wind 10 m/s*

4.2.2 Finer Mesh Regions at 4 cm Downstream

In this section, regions investigated with a finer mesh are presented and compared with the corresponding areas measured with the coarser mesh and from a CFD simulation.

Figure 4.23: *Zoom on the right strut with varying depth*

Figure 4.24: *Zoom on the lower strut with uniform depth*

Figure 4.25 and 4.27 shows the streamwise velocity component for the cases with a wind velocity of 5 m/s and a fan rotation of 1400 and 2800 rpm in the zoomed-in region on the strut positioned at the right hand side behind the fan. This strut has a greater depth on the half close to the hub and at the tip with a narrower section in between, see Figure 4.23, compare to the lower strut with uniform depth in Figure 4.24. This nonuniform shape justifies why the highest velocities appear above and below the strut in the near hub region. The case with a rotation speed of 2800 rpm causes high velocities at tip radius behind the strut that does not seem to occur for the 1400 rpm case. Downstream the narrow section of the strut the flow shows a slight upward curve, that deviates from the shape of the strut, due to the counter clockwise rotation of the fan.

For comparison, to see how the measured velocity field changes when increasing the mesh resolution, the corresponding regions from the coarse measurements of the downstream flow field is illustrated in Figure 4.26 and 4.28. The coarse mesh in this region is measured with only 38 points compared to 609 measurement points for the fine mesh. As one can see, the regions behind the strut shows lower velocities for the measurements with a finer mesh compared to the coarse mesh which has a more smeared out velocity field. For the 2800 rpm case the coarse measurement does not seem to be able to capture the region with high velocities just above the strut at tip radius. The reason for the lower accuracy for the coarse measurement is due to the cubic interpolation between the more scattered points.

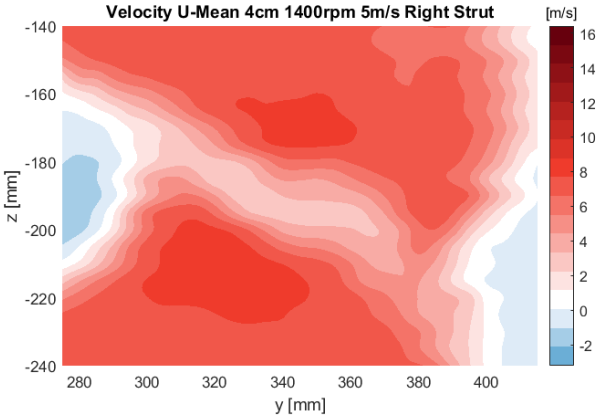

Figure 4.25: *Right strut streamwise velocity fan rotation 1400 rpm, wind 5 m/s*

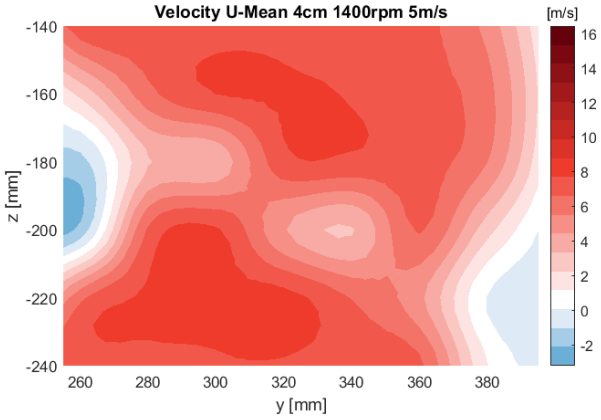

Figure 4.26: *Coarse mesh right strut streamwise velocity fan rot. 1400 rpm, wind 5 m/s*

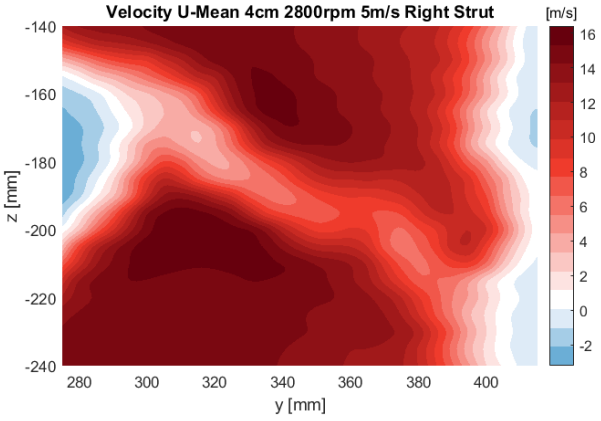

Figure 4.27: *Right strut streamwise velocity fan rotation 2800 rpm, wind 5 m/s*

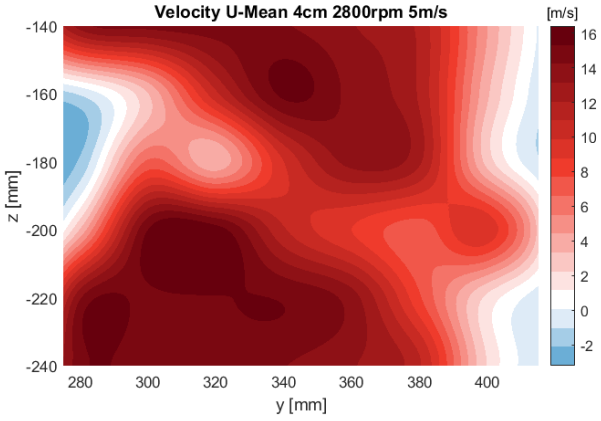

Figure 4.28: *Coarse mesh right strut streamwise velocity fan rot. 2800 rpm, wind 5 m/s*

Figure 4.29 shows the corresponding case from a CFD simulation. As one can see the the velocity field looks very similar to the measurement with the fine mesh. In the region just above the strut at tip radius, the fine mesh and CFD plots show a region with high velocities that is not captured by the coarse mesh.

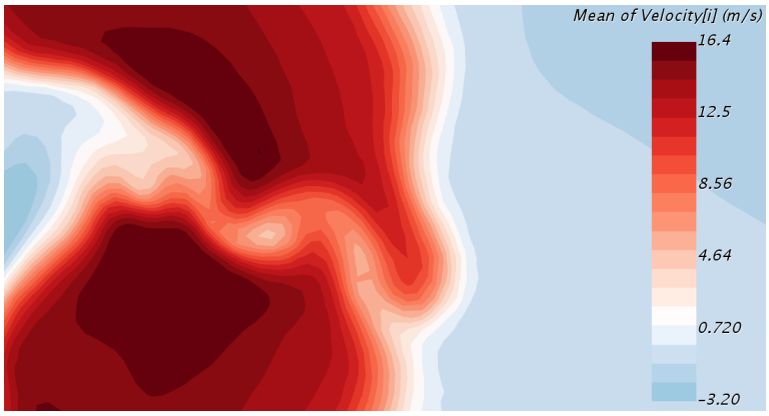

Figure 4.29: *Zoom the the right strut from a CFD simulation*

For the vertical cross-stream velocity the highest velocities appear near the hub and tip radius of the blades just below the strut, as shown in Figure 4.30 and 4.32. The measurements with a coarse mesh, in Figure 4.31 and 4.33, are not able to capture as high velocities and shows a flow field with slightly underestimated velocities.

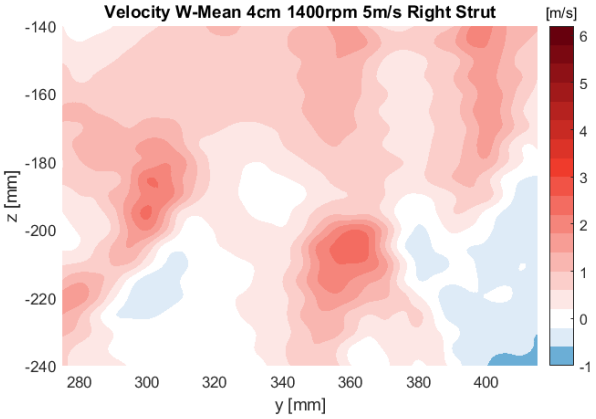

Figure 4.30: *Right strut vertical cross-stream velocity fan rotation 1400 rpm, wind 5 m/s*

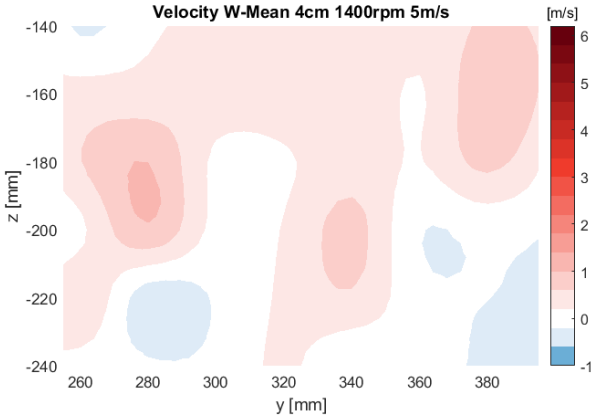

Figure 4.31: *Coarse mesh right strut vertical cross-stream velocity fan rot. 1400 rpm, 5 m/s*

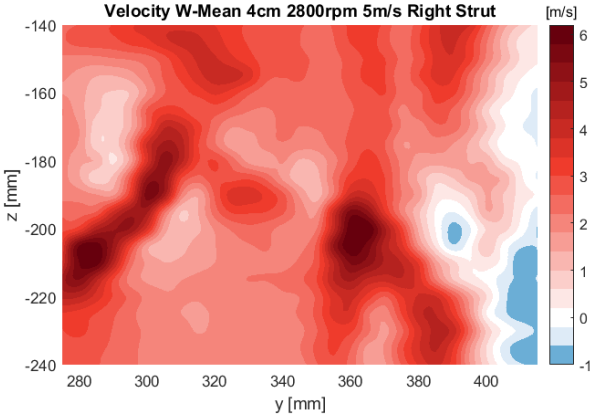

Figure 4.32: *Right strut vertical cross-stream velocity fan rotation 2800 rpm, wind 5 m/s*

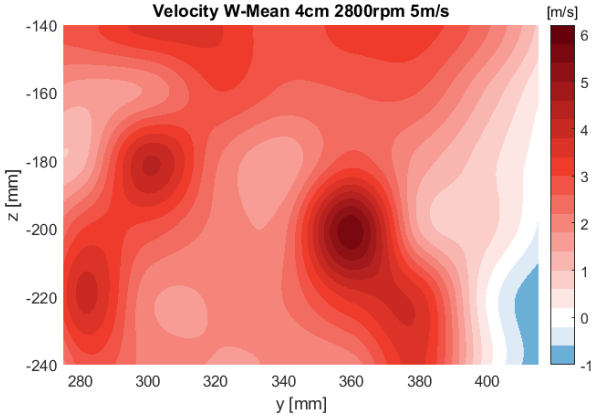

Figure 4.33: *Coarse mesh right strut vertical cross-stream velocity fan rot. 2800 rpm, 5 m/s*

Figures 4.34 and 4.35 show the velocity field downstream of the lower strut, which has a uniform depth, see Figure 4.24 above. In comparison with the right strut, the higher velocity seems to be more evenly distributed over the blade span. This further implies that the occurrence of the highest velocities near the hub for the right strut is a cause of its non-uniform depth. Similarly to the right strut in Figure 4.32, the maximum positive cross-stream velocities occur at hub and tip radius. However, with a smaller magnitude (note the velocity scale difference) since the upward directed velocities clearly will be higher over the right horizontal strut following the rotation of the fan. The largest velocities in negative direction occur over the blade span on the left side of the measured region where the centrifugal force from the fan rotation drives the flow downwards and the blockage of the strut has not yet redirected the flow.

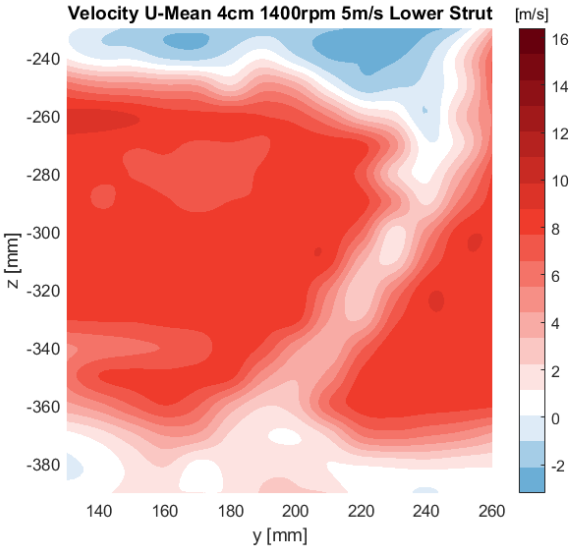

Figure 4.34: *Lower strut streamwise velocity fan rotation 1400 rpm, wind 5 m/s*

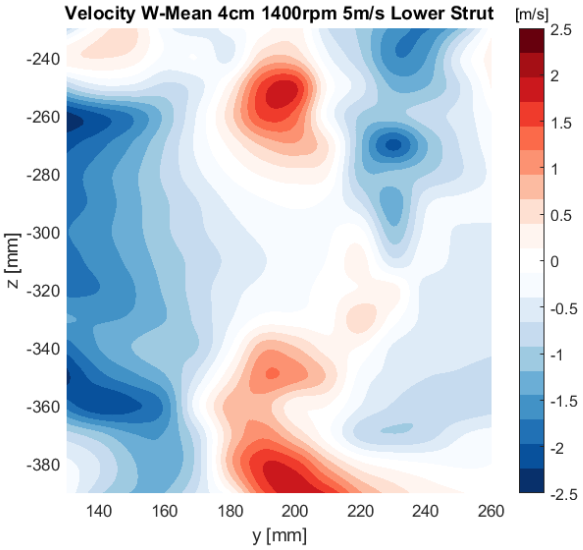

Figure 4.35: *Lower strut vertical cross-stream velocity fan rotation 1400 rpm, wind 5 m/s*

The streamwise velocity field behind the control module for 1400 and 2800 rpm and a wind tunnel speed of 5 m/s is shown in Figure 4.36 and 4.38. As one can see, the increase of fan rotation speed gives maximum velocities almost twice as high but with a very similar flow behaviour. For both cases the highest velocities occur in the area between the left strut and the control modules lower end where the flow accelerates through the smaller area to maintain the massflow. The measurements with the coarser mesh, shown in Figure 4.37 and 4.39, give a more smeared out visualization with slightly lower velocities. The biggest differences occur in the area below the control module where the curved region with high velocities is not captured by the coarse mesh.

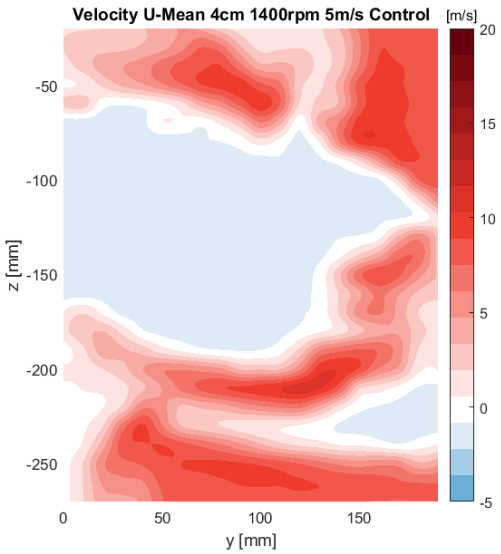

Figure 4.36: *Fine mesh control module streamwise velocity fan rotation 1400 rpm, wind 5 m/s*

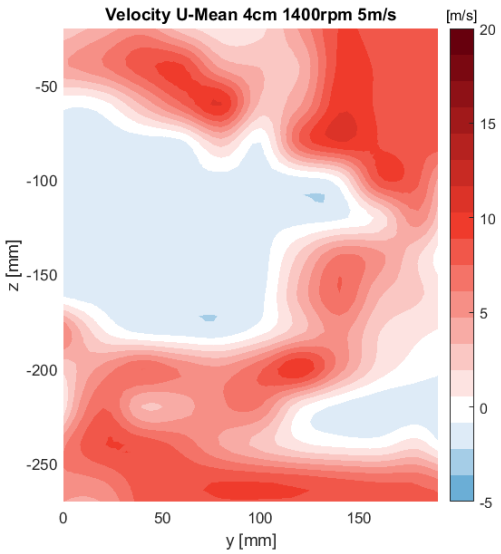

Figure 4.37: *Coarse mesh control module streamwise velocity fan rotation 1400 rpm, wind 5 m/s*

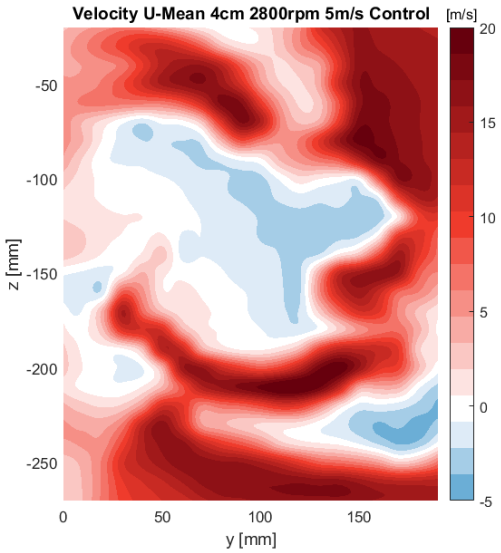

Figure 4.38: *Fine mesh control module streamwise velocity fan rotation 2800 rpm, wind 5 m/s*

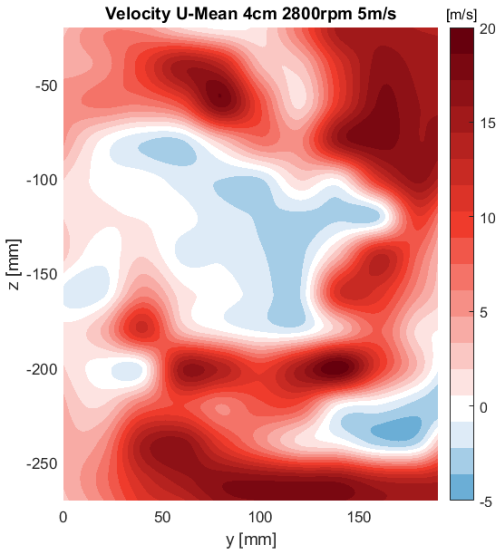

Figure 4.39: *Coarse mesh control module streamwise velocity fan rotation 2800 rpm, wind 5 m/s*

In Figure 4.40 the velocity field from CFD is shown for the case with a fan rotation of 2800 rpm and a wind velocity of 5 m/s. The color scale differs slightly from the Matlab generated plots but it is clear that the control module region measured with the fine mesh gives the flow prediction qualitatively closest to the CFD simulation.

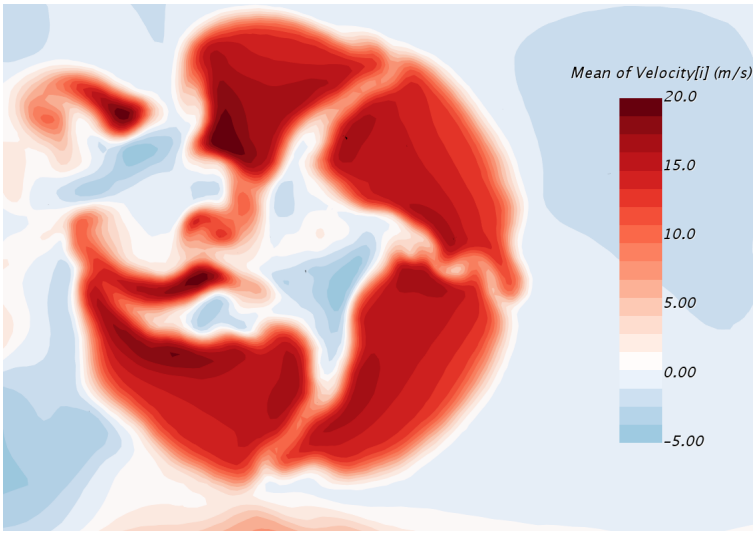

Figure 4.40: *Streamwise velocity field from CFD*

For the vertical cross-stream velocity the region downstream the control module is around 0 m/s for the 1400 rpm case as shown in Figure 4.41. The region above has an upward moving flow due to blockage and the region below have downward directed velocities following the fan rotation. Increasing the fan rotation speed to 2800 rpm gives a larger region with velocities in negative z-direction closer to the hub, see Figure 4.43.

As for the previous comparisons, the interpolation between the points in the coarse mesh gives a slightly lower velocity field then the fine mesh, especially for the 1400 rpm case, as one can see in Figure 4.42 and 4.44.

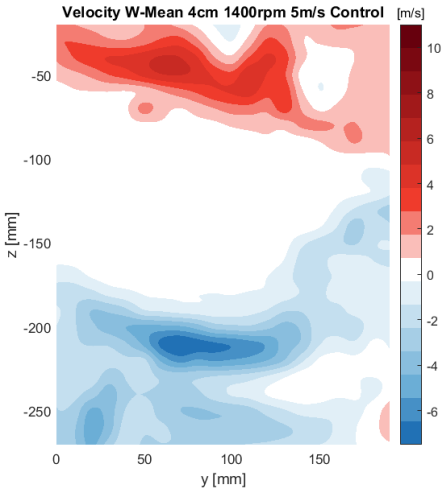

Figure 4.41: *Fine mesh control module vertical cross-stream velocity fan rotation 1400 rpm, wind 5 m/s*

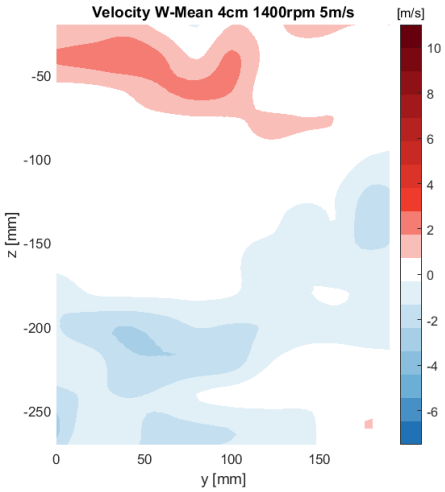

Figure 4.42: *Coarse mesh control module vertical cross-stream velocity fan rotation 1400 rpm, wind 5 m/s*

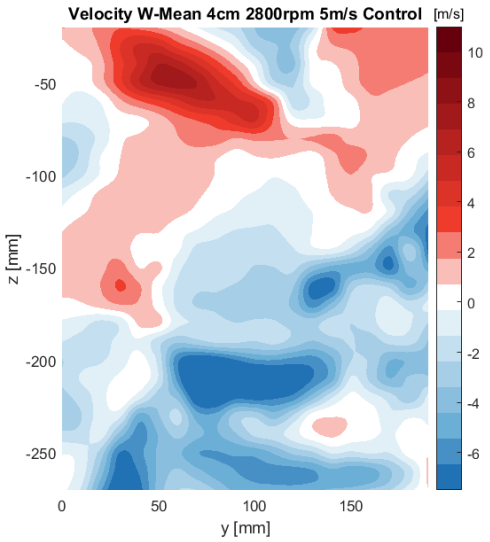

Figure 4.43: *Fine mesh control module vertical cross-stream velocity fan rotation 2800 rpm, wind 5 m/s*

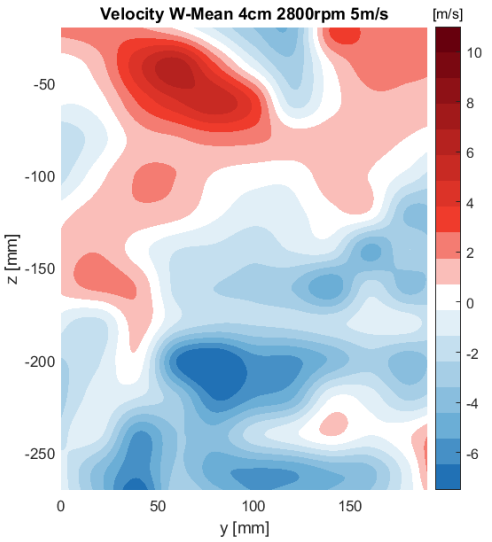

Figure 4.44: *Coarse mesh control module vertical cross-stream velocity fan rotation 2800 rpm, wind 5 m/s*

4.2.3 Horizontal Cross-Stream Velocity Component

Plots of the velocity field from measurements with the probe in a vertical position, obtaining the streamwise and horizontal cross-stream direction, are presented below. The plots on the left side for the streamwise velocity should, if the probe was positioned correctly, be equal to the ones presented in section 4.2.1 and will therefore not be discussed here. (The plots for the streamwise velocity should, if the probe was positioned correctly, be equal to the ones presented in section 4.2.1 and will therefore not be discussed here. (to verify that the probe was placed correctly after being redirected, A comparison of the streamwise velocity field plots obtained with the probe in horizontal and vertical position is shown in Figure 4.45 and 4.46))

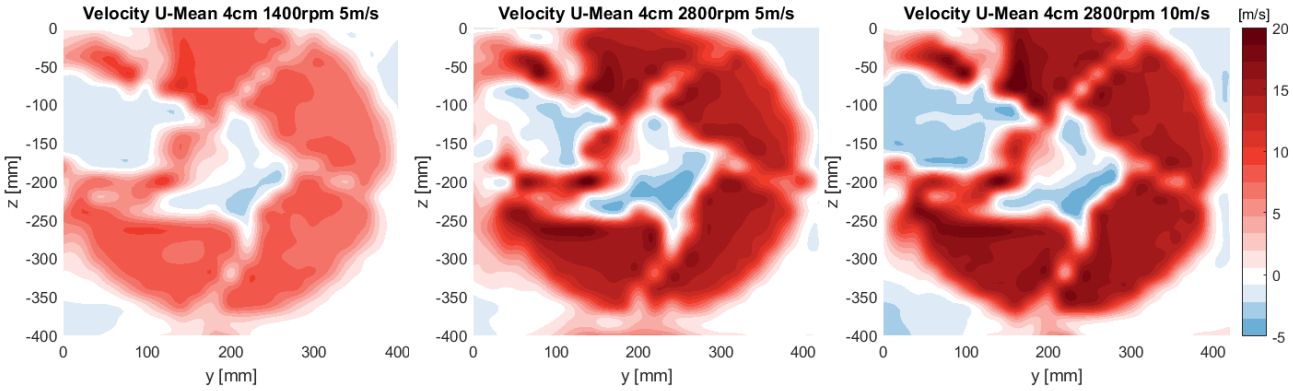

Figure 4.45: *Streamwise velocity fan rotation 1400 rpm wind 5m/s (left), 2800rpm wind 5 m/s (middle) and 2800 rpm wind 10 m/s (right) at 4 cm downstream*

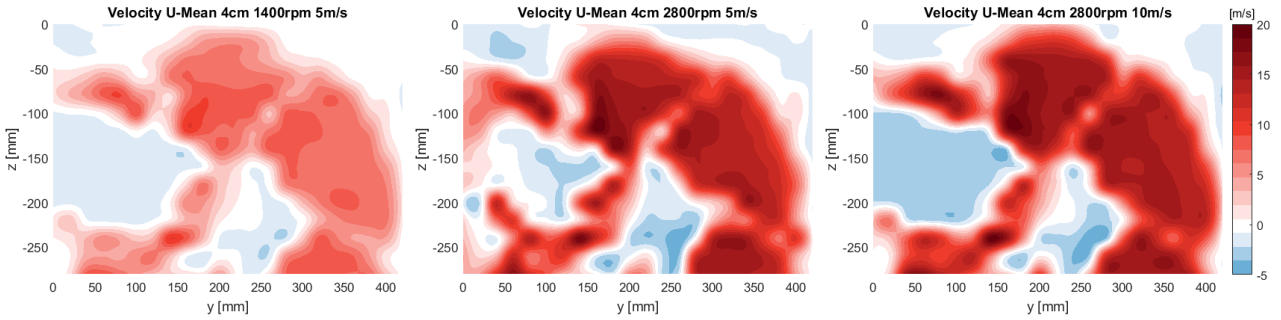

Figure 4.46: *Upper half streamwise velocity fan rotation 1400 rpm wind 5 m/s (left), 2800 rpm wind 5 m/s (middle) and 2800 rpm wind 10 m/s (right) at 4 cm downstream*

Figure 4.47 shows the velocity components in horizontal cross-stream direction for the case with a wind tunnel speed of 5 m/s and a fan rotation of 1400 rpm. The region downstream of the blade span seems to be characterized by slightly negative velocities, directed to the left. The left and upper regions are characterized by velocities acting to the left due to the fan's rotation. The velocities in the middle region are acting in the opposite direction, possibly due to the inward turning effect around the fan engine.

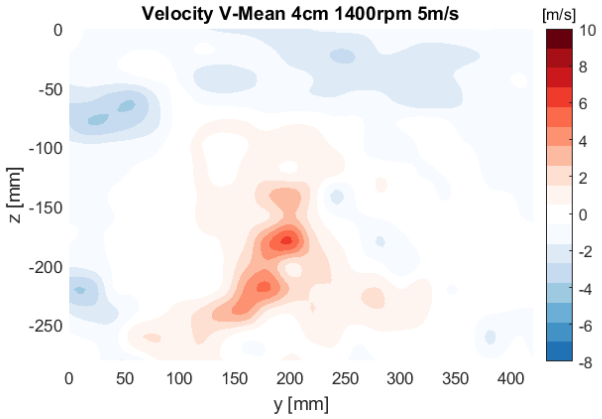

Figure 4.47: *Upper half horizontal cross-stream velocity fan rotation 1400 rpm, wind 5 m/s*

With the fan rotation increased to 2800 rpm the regions with negative velocities will be more pronounced, shown in Figure 4.48. The region downstream of the control module mainly consists of flow going in positive y-direction due to the forward swept blades.

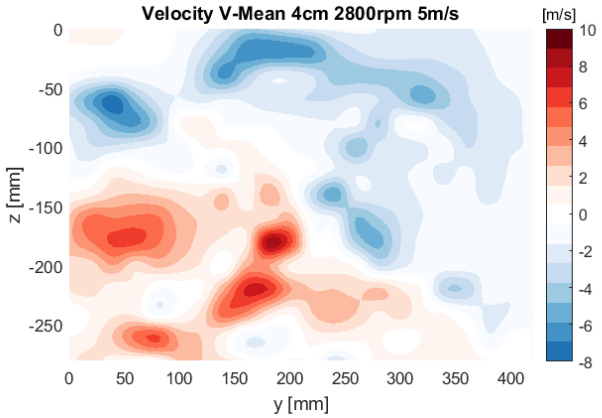

Figure 4.48: *Upper half horizontal cross-stream velocity fan rotation 2800 rpm, wind 5 m/s*

When increasing the wind tunnel velocity to 10 m/s (see Figure 4.49) the positive velocities seems to be forced towards the middle and velocities directed outwards occur on the left side, very similar to the case shown in Figure 4.47 but with larger magnitude.

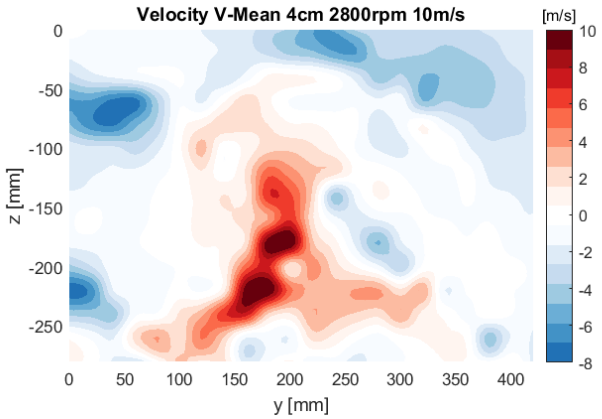

Figure 4.49: *Upper half horizontal cross-stream velocity fan rot. 2800 rpm, wind 10 m/s*

4.2.4 Further Downstream Measurements

For the measurements at the planes 8 and 12 cm downstream the velocity plots shows a similar flow behaviour but are generally more smeared out as the dissipation of the flow increases with the downstream loss in momentum. Therefore, only a general description of the downstream flow behaviour will be presented and particularly the plots for the cases where the flow field appeared to be significantly different, visualized. All plots of the velocity field from the planes 8 and 12 cm downstream can be found in A Appendix.

Streamwise

Overall, the blockage by the control module seems to have an increased impact on the streamwise flow further downstream causing larger regions with reversed flow for the streamwise velocity component. The streamwise velocities in the regions around the control module are decreasing with increasing downstream distance due to the deceleration of the flow approaching the wind tunnel flow speed. As presented earlier, at 4 cm downstream the fan, the acceleration through the confined spaces around the control module causes the highest velocities. However, at 12 cm downstream the control module these high velocities has been heavily reduced. Also, the influence of the struts on the flow field can hardly be distinguished this far downstream, as illustreated in Figure 4.50.

The centre region with reversed flow becomes smaller and smaller mostly due to the inward turning flow between the control module and the motor. Especially for the 2800 rpm case, the flow between the control module and motor moves towards the middle following the right directed flow noticed for the horizontal cross-stream component at 4 cm downstream in section 4.2.3.

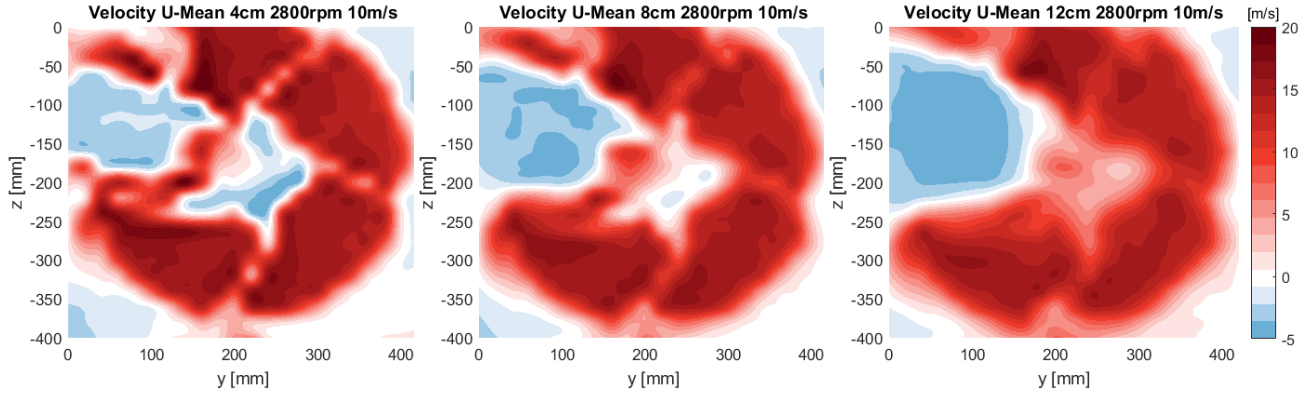

Figure 4.50: *Comparison of streamwise velocity fan rotation 2800 rpm wind 10 m/s at 4 cm (left), 8 cm (middle) and 12 cm (right) downstream*

Figure 4.51 shows a comparison between the case with only wind velocity of 10 m/s and only fan rotation of 1400 rpm. Even though the case with only wind caused a fan rotation of around 1200 rpm the flow behaviour shows a very different behaviour with a stronger spreading in radial direction. The higher velocities for the only wind case could be motivated by the high velocity moving air flow circulating in the tunnel compared to the case only driven by fan, where stagnant air is sucked through the fan. However, as mentioned earlier, the case with just power supply driving the fan had a less distributed seeding, influencing the flow field.

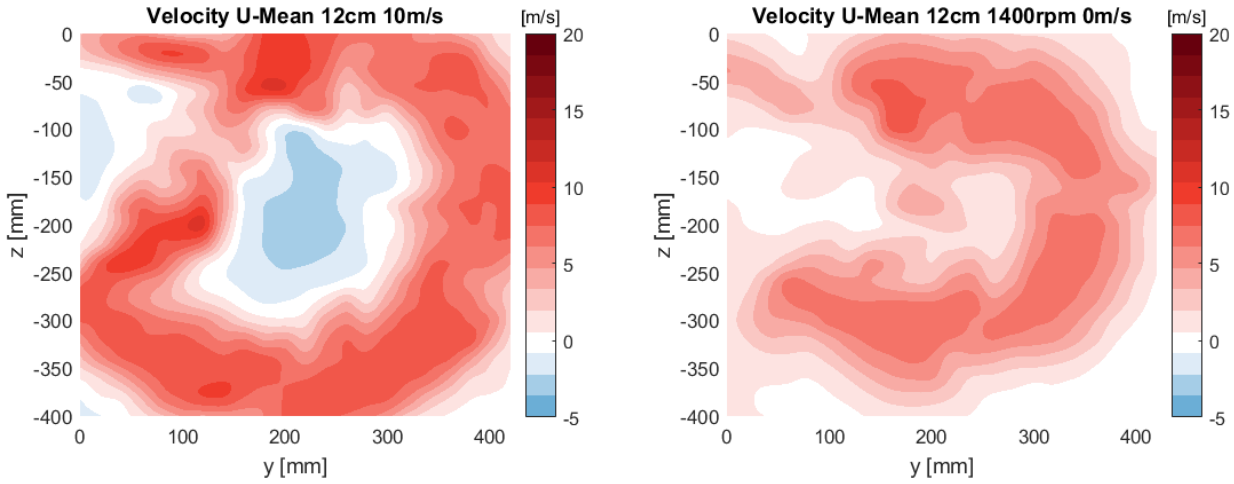

Figure 4.51: *Comparison of streamwise velocity for 10 m/s wind speed and no forced fan rotation (left) and 1400 rpm fan rotation and no wind speed (right)*

In general, as for the plane 4 cm downstream, the streamwise velocity field seems to spread vertically in a higher degree than in horizontal direction due to the lower blockage at the top and bottom then on the sides. This is shown for the cases at 12 cm downstream with a fan rotation of 2800 rpm and a wind velocity of 0, 5 and 10 m/s in Figure 4.52.

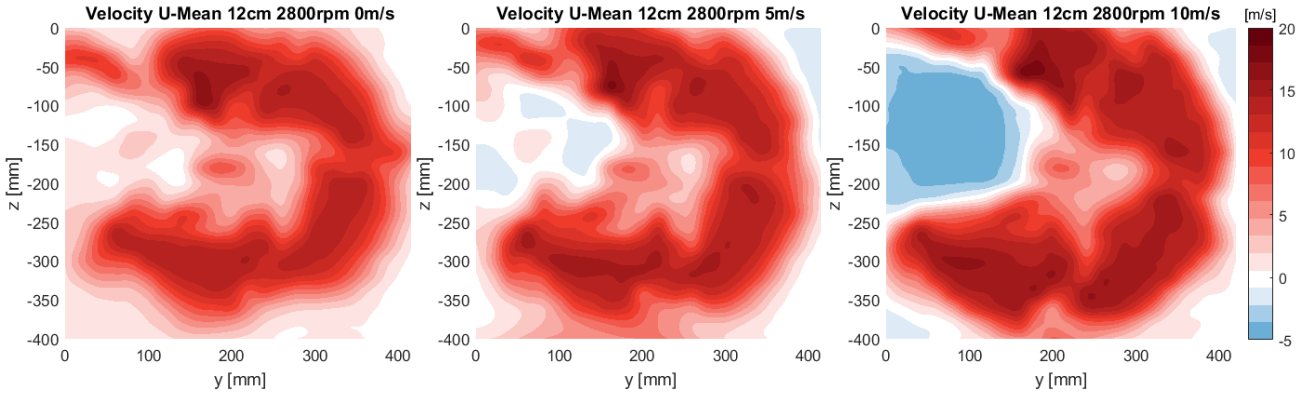

Figure 4.52: *Comparison of streamwise velocity at 12 cm downstream and a fan rotation of 2800 rpm for wind velocities of 0 m/s (left), 5 m/s (middle) and 10 m/s (right)*

Vertical Cross-Stream

The vertical velocity component at 8 and 12 cm downstream of the fan shows a similar flow behaviour for 2800 rpm as for the 4 cm upstream plane. The cases with a fan rotation speed of 1400 rpm, on the other hand, show larger velocities directed upwards and downwards with increasing downstream distance. This arises since the flow that has been decreased passing through the rotating fan is again accelerated up to the wind tunnel air flow velocity. This downstream comparison is shown in Figure 4.53 for the case with a wind velocity of 10 m/s and a fan rotation speed of 1400 rpm.

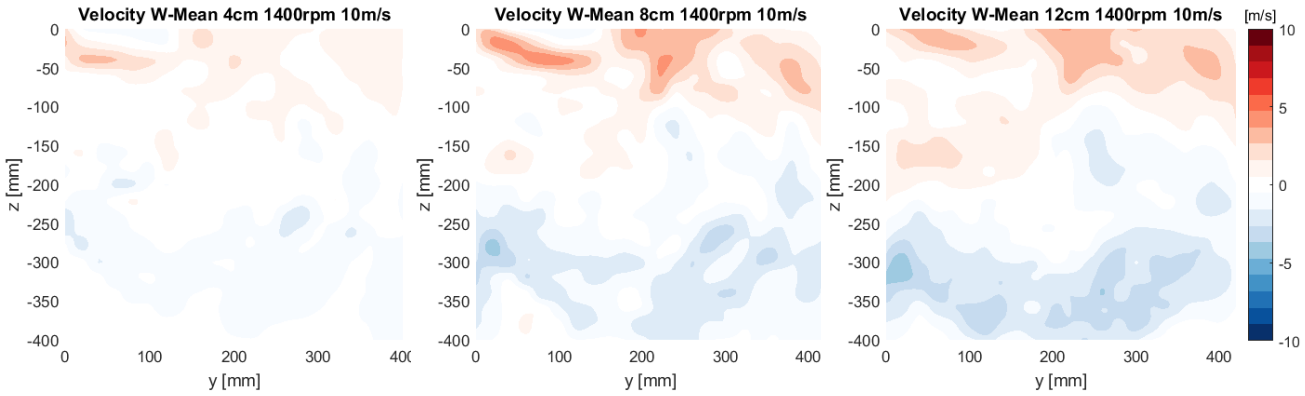

Figure 4.53: *Comparison of vertical cross-stream velocities for fan rotation 1400 rpm and wind 10 m/s at 4 cm (left), 8 cm (middle) and 12 cm (right) downstream*

4.2.5 Spectral Analysis

Figures 4.54, 4.55 and 4.56 illustrate the frequency spectrum over the blade span at the hub, midspan and tip radius respectively. The positions are measured in radial direction over the blade span between the lower and right struts. The clear peaks correspond to the fan rotation frequency of 46.97 Hz, calculated from the average rotation speed for this case, 2818 rpm divided by 60 seconds, and its following harmonics. At hub and tip radius the amplitude of the dominant frequencies is larger than at midspan but the signals contain more noise. This due to the impact of the surrouding geometry at these locations, the shroud at the tip and the engine at the hub. At midspan, where less flow disturbance occur, the flow fluctuates less and the gives a lower amplitude frequency spectrum. At the tip only the first peak of the fan rotation frequency appear as dominant. A possible explanation to this could be the higher fan momentum with increasing radius. The other dominant peak occurring at approximately 376Hz, for the hub and midspan measurements, is the blade passing frequency, which is the fan rotation frequency times the number of blades (46.97*8=375.8Hz).

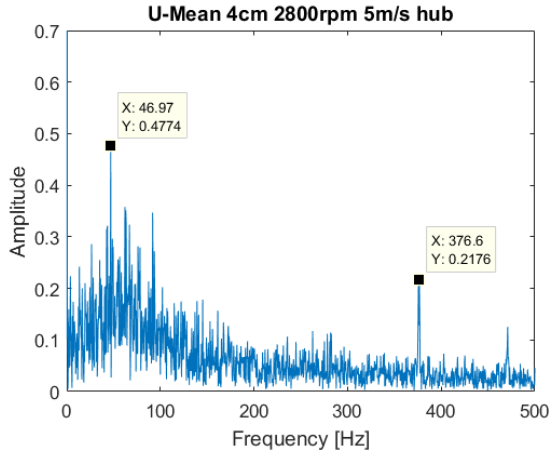

Figure 4.54: *Frequency spectrum 4 cm downstream, streamwise velocity fan rotation speed 2800 rpm and 5 m/s wind at hub radius*

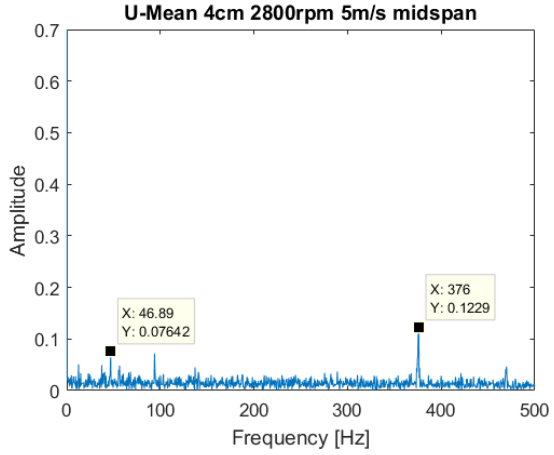

Figure 4.55: *Frequency spectrum 4 cm downstream, streamwise velocity fan rotation speed 2800 rpm and 5 m/s wind at mid radius*

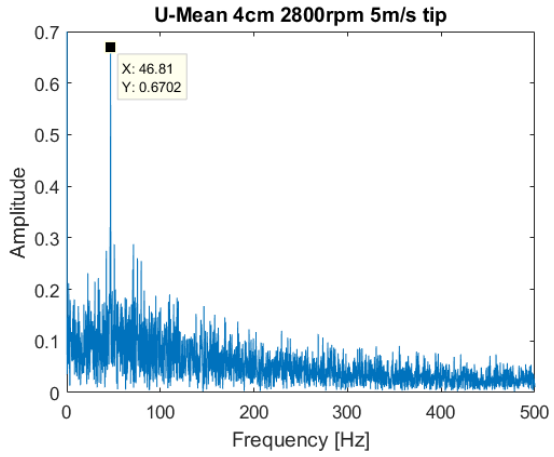

Figure 4.56: *Frequency spectrum 4 cm downstream, streamwise velocity fan rotation speed 2800 rpm and 5 m/s wind at tip radius*

4.2.6 Uncertainties of Results

When performing physical measurements, the presence of uncertainties and errors are unavoidable. Possible reasons for these can be the experimental equipment, the measuring process, the investigated object, or originate from the environment. Below, the measurement uncertainties that might have caused errors will be presented and discussed.

In this study the construction holding the fan may not have been perfectly normal to the flow. The horizontal and vertical alignment when mounting the probe was measured with respect to the wind tunnel walls but may not have been completely correct positioned. Also the probe position for the laser beams, measuring the velocities in the three different directions was judged by eye so it may not have been completely aligned with the coordinate axis.

Especially for the measurements with a fan rotation of 2800 rpm the probe could be seen vibrating. This issue was hard to remove since the traverse mounting for the cylinder, at which the probe is attached, was a little bit loose. Also the quite stiff fibre optics cable to the probe could have been contributing to the vibrations, since it was not possible to tape it tight to the traverse arm. The highest fan rotation speed also caused the entire construction for mounting the fan to vibrate slightly. These low amplitude vibrations could be sensed but not detected by eye due to the rigid fastening of the steel construction and were not possible to remove.

With the manual control of the fan rotation speed by the power supply and PWM-controller it was difficult to set the exactly same rotation speed for the different cases as a specific percentage by the PWM-controller did not always generate the same rotation speed. By slightly changing the voltage and current similar rotations could be set at the start of each test but the rotation speed was varying during the measurement. The reason for this was most likely the unsteadiness in the wind tunnel operation. The wind tunnel velocity variation for different freestrem velocities can be seen in B Appendix. The variation of rotation speed for the different cases can be seen in Table 4.2. Note that the measurements of the rotation speed were mainly just to check that the rotation per minute not deviated too much from the desired value and the amount of measurements and time between measurements differ from case to case (in average 8-10 measurements per case).

Table 4.2: Average fan rotation speed for the different measured cases

Case	[rpm]	4cm	8cm	12cm
1400rpm, 5m/s	Average	1414	1418	1419
	Std dev	17.3	6.6	3.6
1400rpm, 10m/s	Average	1411	1400	1397
	Std dev	0.6	14.7	7.0
2800rpm, 5m/s	Average	2818	2812	2815
	Std dev	6.8	6.7	3.4
2800rpm, 10m/s	Average	2806	2814	2799
	Std dev	2.9	3.3	6.7
1400rpm, 0m/s	Average		1409	1399
	Std dev		4.5	8.1
2800rpm, 0m/s	Average	2817	2788	2806
	Std dev	2.2	1.0	6.3
10m/s	Average	1232	1187	1212
	Std dev	1.4	45.0	37.3
5m/s	Average	163		
	Std dev	67.5		

For the case with a freestream velocity of 5 m/s and no forced fan rotation, the rotation varies with about 40 %. The the maximum rotation speed for this case was 225 rpm but sometimes the fan did not rotate at all. The reason for this is as mentioned the unsteady behaviour of the wind tunnel when operating with this low speed. Therefore this case was not included in the further investigation at the planes 8 and 12 cm downstream of the fan. When increasing the wind velocity to 10 m/s the fan rotations varied less, following the more stable behaviour of the wind tunnel. In Figure 4.57 the variation of wind tunnel velocity is shown. The blue line is the mean velocity and the yellow and orange shows the standard deviation. As one can see, wind speeds over 4 m/s has a lower velocity variation.

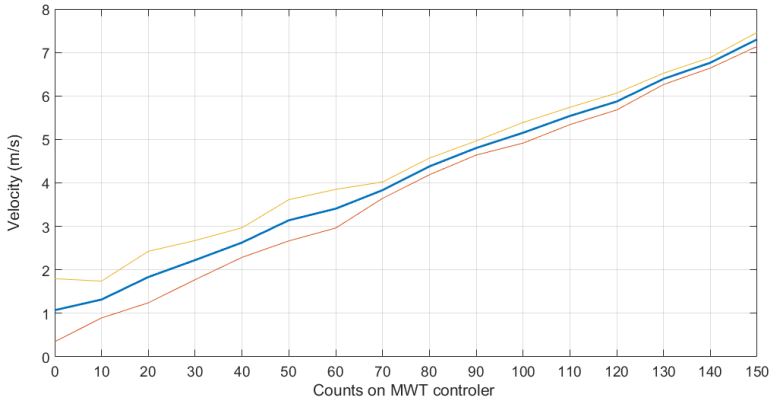

Figure 4.57: *Velocity over counts on controler, i.e. the velocity variation with increasing air speed. The blue line illustrates the velocity and the yellow and orange lines shows the upper and lower limits of the standard deviation.*

When the objective is to obtain averaged quantities as mean and RMS velocity it is preferred to gain at least 1000 particle samples at each position. This was not fulfilled at all positions due to flow blockage, seeding density and photo-multiplier quality. In Figure 4.58 one can clearly see the influence of the shroud and control module blockage on the particle count for the case with a rotation speed 1400 rpm and a wind tunnel speed of 5 m/s, at the plane 8 cm downstream. The region over the blade span where high streamwise velocities occur is likewise the area with the highest particle count both in streamwise- and vertical cross-stream direction. It was especially hard to achieve a high particle count in the directions normal to the flow, i.e. measuring the vertical and horizontal cross-stream velocity components, where the count was below 1000 samples at several positions. This could be due to that an old photo-multiplier was used in these measurement directions.

With the smoke machine controlled by a remote, the time between each burst of smoke were not continuously the same, which can have contributed to an uneven seeding density in the tunnel.

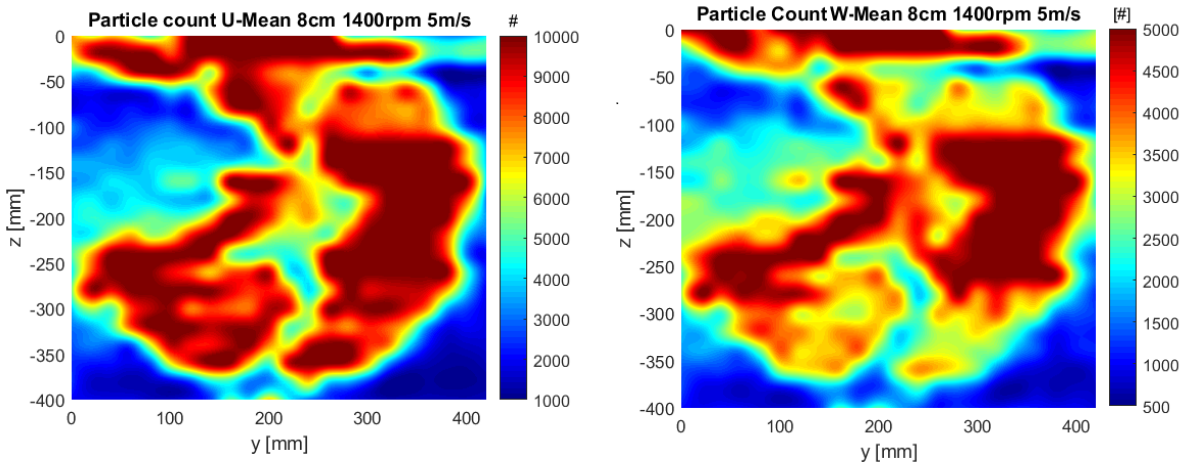

Figure 4.58: *Particle count in streamwise direction, U (left) and vertical cross-stream direction, W (right)*

Due to the time limitation, the measurements were only performed one time, for the best results repeated measurements should have been performed on the same positions and then calculating an average. Since the wind tunnel conditions, fan rotation speed, seeding density varies over time there will seemingly be some variation of the measured velocities as well. Only one measurement at each position could lead to errors only noticeable when comparing with repeated measurements. If it was detected during test that the measurement at some point was giving a nonphysical value, due to for example too low particle count from poor seeding, this point was repeated for better comparison.
To quantify the error from single velocity measurements, four test measurements were performed across the middle of the fan in y-direction for the case with a wind tunnel speed of 10 m/s and fan rotation of 2800 rpm at 4 cm downstream. The result from the measurements is shown in Table 4.3 where the mean streamwise velocities in m/s is shown together with the average and standard deviation at each point. The corresponding results in the vertical cross-stream direction is presented in Table 4.4. Overall the cross-stream velocity measurements show a slightly higher standard deviation compared to

the streamwise velocity measurements. Since there is no specific trend of where in the wake large or small standard deviations occur it is difficult to draw a verdict about the behaviour of the velocity variation.

Table 4.3: Repeated tests streamwise velocity [m/s]

Test 1	Test 2	Test 3	Test 4	Average	Std deviation
2.52	2.32	2.30	2.26	2.35	0.12
4.19	3.99	4.20	4.14	4.13	0.10
10.42	10.58	10.52	10.63	10.54	0.09
13.29	13.67	13.99	13.86	13.70	0.30
10.12	9.96	10.69	10.74	10.38	0.40
6.32	6.07	6.12	6.24	6.19	0.11
12.02	12.24	12.36	12.49	12.28	0.20
20.35	20.61	20.58	20.54	20.52	0.12
11.97	12.01	12.09	12.39	12.12	0.19
1.59	1.38	1.43	1.45	1.46	0.09
0.58	0.63	0.30	0.27	0.45	0.19
-1.38	-1.53	-1.35	-1.45	-1.43	0.08
-2.73	-2.84	-2.87	-2.80	-2.81	0.06
-4.35	-4.49	-4.34	-4.42	-4.40	0.07
-3.16	-3.15	-3.56	-3.43	-3.33	0.20
11.59	11.93	12.03	12.03	11.90	0.21
15.09	15.34	15.18	15.13	15.19	0.11
9.01	9.25	9.17	9.22	9.16	0.11
6.96	7.12	6.52	6.83	6.86	0.25
13.76	14.01	13.85	13.73	13.84	0.13
3.79	4.11	4.98	4.53	4.35	0.52

Table 4.4: Repeated tests cross-stream velocity [m/s]

Test 1	Test 2	Test 3	Test 4	Average	Std deviation
3.12	3.15	3.79	3.54	3.40	0.32
5.24	5.23	5.97	5.95	5.60	0.42
7.26	8.31	8.68	9.32	8.39	0.86
8.95	9.55	10.07	10.01	9.65	0.52
7.55	7.36	7.90	8.86	7.92	0.67
4.90	5.40	5.53	5.73	5.39	0.35
5.80	6.42	6.81	6.39	6.36	0.42
5.68	5.93	5.84	6.43	5.97	0.32
4.19	4.30	4.41	4.09	4.25	0.14
1.77	1.96	1.66	2.09	1.87	0.19
2.57	2.93	2.65	2.23	2.60	0.29
1.46	1.72	1.46	1.76	1.60	0.16
2.33	2.36	2.66	2.46	2.45	0.15
2.28	2.22	2.71	2.57	2.45	0.23
-0.53	-0.72	-0.50	-0.17	-0.48	0.23
-3.43	-3.68	-3.59	-4.05	-3.69	0.26
0.02	0.16	0.02	0.18	0.10	0.09
-1.90	-2.05	-2.35	-1.78	-2.02	0.25
-1.92	-1.68	-1.62	-2.00	-1.81	0.18
0.30	0.24	0.16	0.24	0.24	0.06
-0.12	-0.23	-0.16	-0.19	-0.18	0.05

5 Conclusion and Future Work

This report presents experimental measurements of the downstream flow behaviour of a cylinder and vehicle cooling fan. The measurements were performed using Laser Doppler Anemometry in a model scale wind tunnel. For the fan measurements, combinations of two different fan rotation speeds, 1400 and 2800 rpm, and two wind tunnel velocities, 5 and 10 m/s, were studied at planes 4, 8 and 12 cm downstream of the fan.

From the initial test measurements performed on a cylinder it can be concluded that in the wake region close to the cylinder it is difficult to get accurate results due to the difficulty to capture a sufficient amount of particles at these positions. Therefore it is important to keep a fairly high density of seeding particles in the wind tunnel to fully show the fluid behaviour. For the spectral analysis of the vortex shedding along the wake centerline, it is difficult to distinguish a clear peak in the frequency spectrum. Further out from the centerline a dominant peak can clearly be detected, at a Strouhal number of approximately 0.2. In comparison with other studies [13, 14] the wake velocity field shows similar characteristics.

The fan measurements indicate that the downstream velocity field is highly dependent on the ratio between wind velocity and fan rotation speed. The highest streamwise velocities for all cases occur in the region around the control module where the blockage and surrounding delimited areas cause an acceleration of the flow. For the velocities in cross-stream direction, the flow is spreading radially outward with increasing downstream distance, forming a conical shaped wake flow. Generally, by increasing the fan rotation speed from 1400 to 2800 rpm the streamwise velocities along the blade span becomes about twice as large. However, downstream of the regions blocked by the motor, control module and shroud, a higher reversed flow appears due to the turning of the flow. Along the blade span the maximum streamwise velocity components are located near the hub for the cases with only air flow driving the fan rotation. With increasing fan rotational speed, by an external power supply, the highest streamwise velocities over blade span seem to move towards the tip. From the spectral analysis, it can be concluded that the largest velocity fluctuations appear at the hub and tip with a lower region at midspan.

Concluding, the LDA system works well together with the wind tunnel and delivers results similar to the ones obtained by CFD simulations. But the current experimental set-up have some limitations. Mainly the unsteady flow in the wind tunnel together with a variation of seeding density can be factors lowering the accuracy of measurements. For future testing the old photo-multipliers, which are the devices used for conversion of the measured light intensity to an electrical signal, should be replaced and the wind tunnel might need some mechanical maintenance for a more stable operation. As the seeding could be confirmed to be a very important part of LDA measurements, it could be a good idea to investigate in a timer for an even particle seeding density. When the object of the measurements is to obtain values for example the mean- and RMS velocities, the results are not that sensitive to small vibrations of the probe. But, when investigating flow frequencies around an object, a rigid positioned probe is desired in order to reduce the noise in the signal. For further testing, the fan induced flow field should be investigated in an actual engine bay or in a simplified model to account for the effects of the surrounding blockage. Just as for all kinds of measurements, there is a constant trade-off between the

time and accuracy of the measurements. Collecting more particles at each position will yield a higher precision of the averaged values but at the expense of very time consuming measurements. LDA should therefore preferably be used to study smaller turbulent flow regions, to maintain a fine mesh without taking too much time, for example downstream a rear view mirror or confined spaces in the engine bay.

Using a larger probe gives the possibility to measure on a longer distance and further reduce the probe caused flow disturbance. The probe can then be placed outside of the wind tunnel, provided that optical access is met.

References

[1] D. Sturtz. *Engine Cooling System*. 2008. URL: https://repairpal.com/cooling-system (visited on 07/09/2018).

[2] J. Law and R. Rennie. *A Dictionary of Physics (7 ed.)* Oxford University Press, 2015. ISBN: 9780198714743.

[3] *Laser Doppler and Phase Doppler Measurement Techniques*. Springer-Verlag Berlin Heidelberg, 2003. ISBN: 978-3-662-05165-8.

[4] D. Y. Babou. *Measurement techniques in fluid dynamics: An introduction 3rd revised edition*. von Karman Institute, 2009. ISBN: 978-2-930389-96-6.

[5] Z. Zhang. *LDA application methods: laser doppler anemometry for fluid dynamics*. Springer-Verlag Berlin Heidelberg, 2010. ISBN: 978-3-642-13514-9.

[6] *LDA and PDA Reference Manual*. Version Publication no.: 9040U1312. Dantec Dynamics A/S, 2011.

[7] *Laser Doppler Anemometry, Introduction to principles and applications*. URL: http://www.ara.bme.hu/neptun/BMEGEATMW03/2017-2018-II/ea-lecture/x02_suda_BMEGEATMW03_Dantec-LDA.pdf (visited on 05/21/2018).

[8] *Measurement principles of LDA*. URL: https://www.dantecdynamics.com/measurement-principles-of-lda (visited on 06/23/2018).

[9] Experimental study of the flow induced by a vehicle fan and the effect of engine blockage in a simplified model. *International Journal of Automotive Technology* **17**.4 (2016), 617–627. DOI: 10.1007/s1223901600616.

[10] Experimental investigation of the 3D unsteady flow field downstream of axial fans. *Flow Measurement and Instrumentation* **17**.5 (2006), 303–314. DOI: 10.1016/j.flowmeasinst.2006.05.002.

[11] A Benchmark Case for Aerodynamics and Aeroacoustics of a Low Pressure Axial Fan (2016).

[12] Experimental Study of Low-Pressure Automotive Cooling Fan Aerodynamics Under Blocked Conditions (2006).

[13] C. Norberg. LDV-measurements in the near wake of a circular cylinder (1998).

[14] C. Norberg. An experimental investigation of the flow around a circular cylinder : influence of aspect ratio. *Journal of Fluid Mechanics* **258**.1 (1994), 287–316. DOI: 10.1017/S0022112094003332.

[15] *Pulse Width Modulation*. URL: https://www.electronics-tutorials.ws/blog/pulse-width-modulation.html (visited on 05/10/2018).

[16] *What is a Pulse Width Modulation (PWM) Signal and What is it Used For?* 2018. URL: https://knowledge.ni.com/KnowledgeArticleDetails?id=kA00Z0000019OkFSAU (visited on 05/10/2018).

[17] *BSA Flow Software User Guide*. Version Build no.: 6.50.00.41. Publication no.: 9040U5747. Dantec Dynamics A/S, 2017.

A Appendix

8cm Downstrean

Streamwise

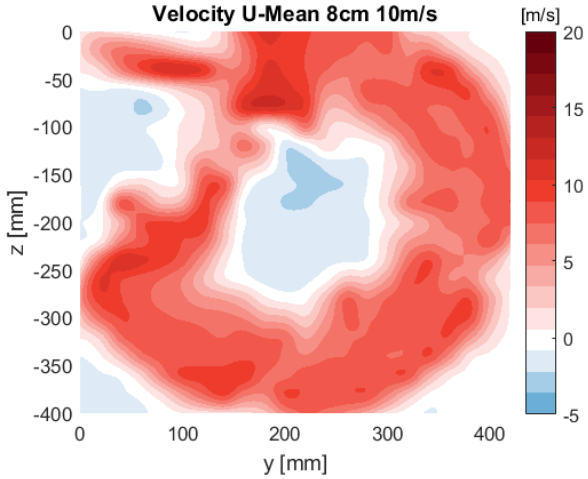

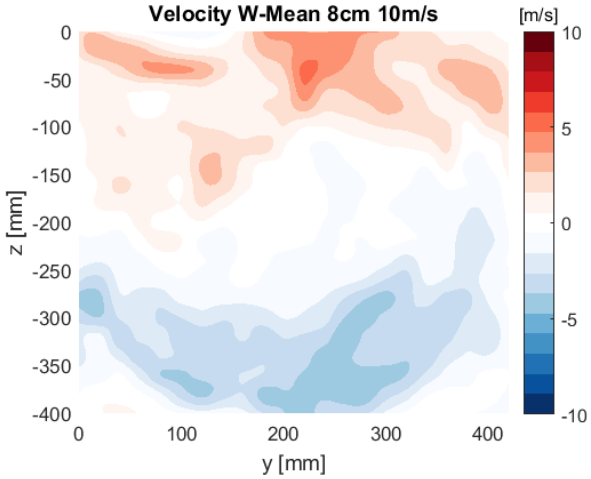

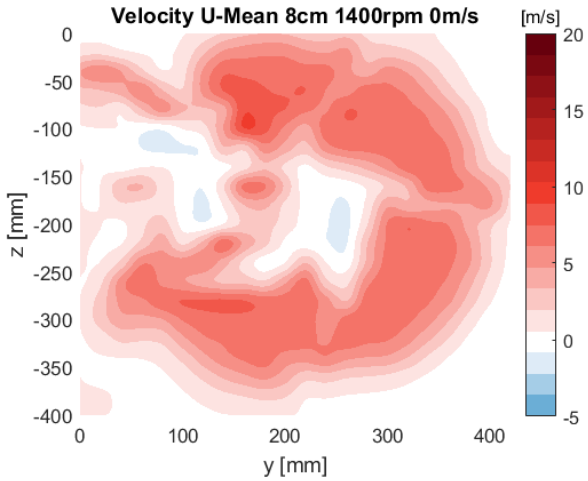

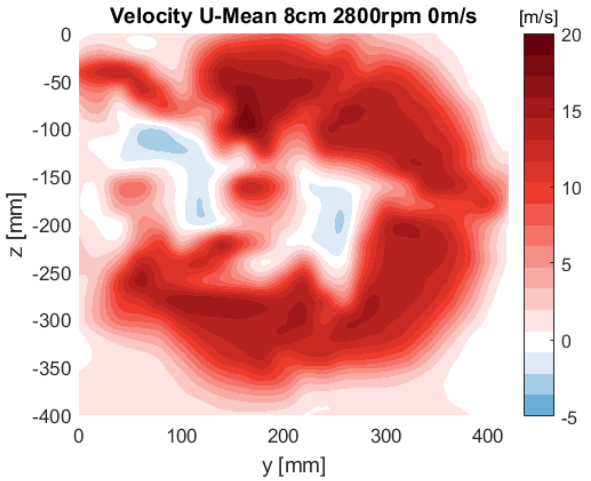

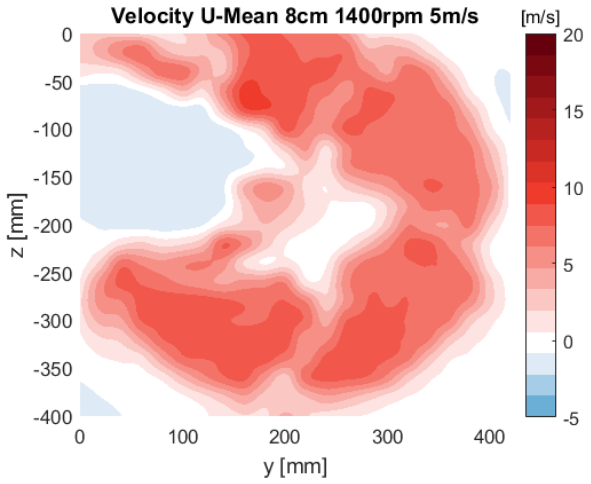

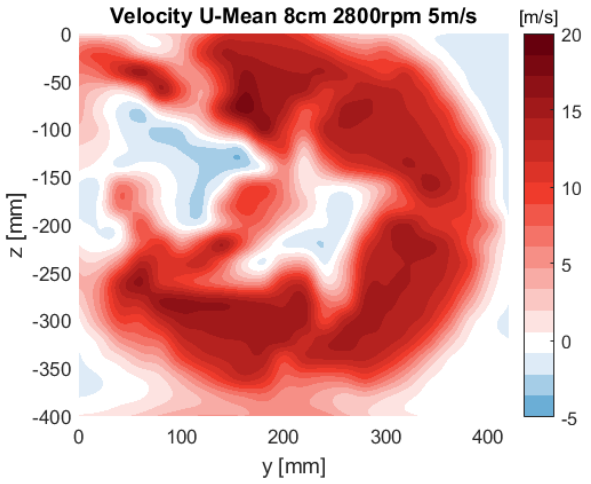

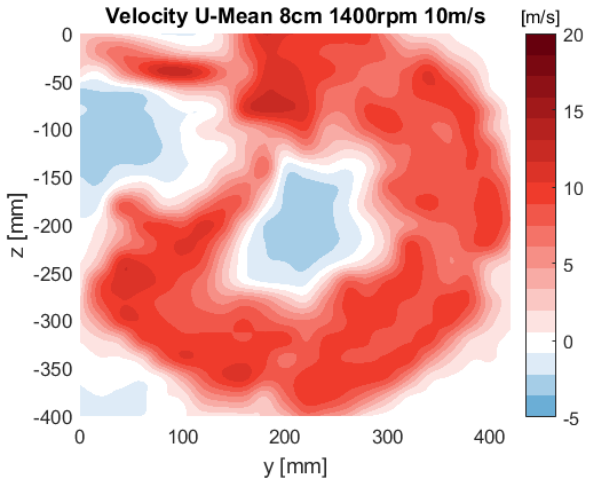

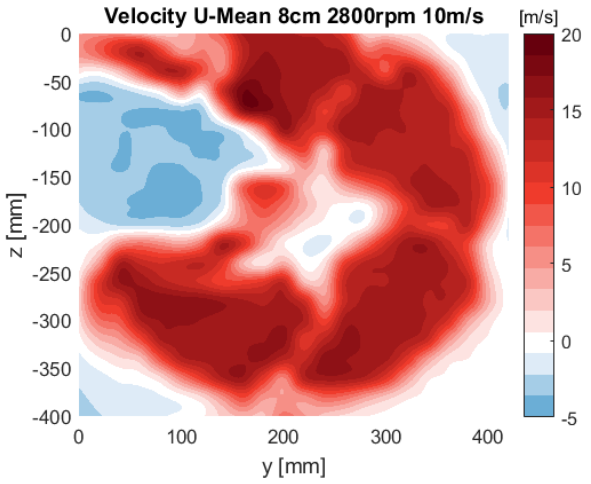

Vertical Cross-Stream

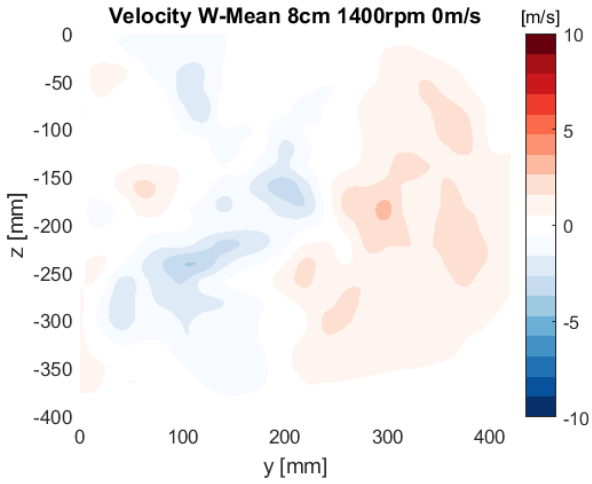

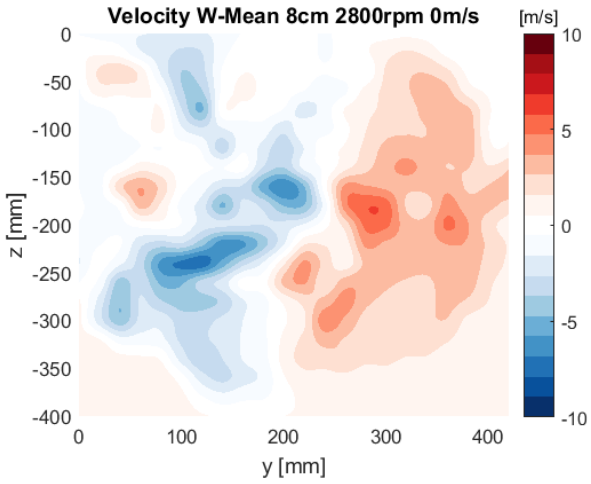

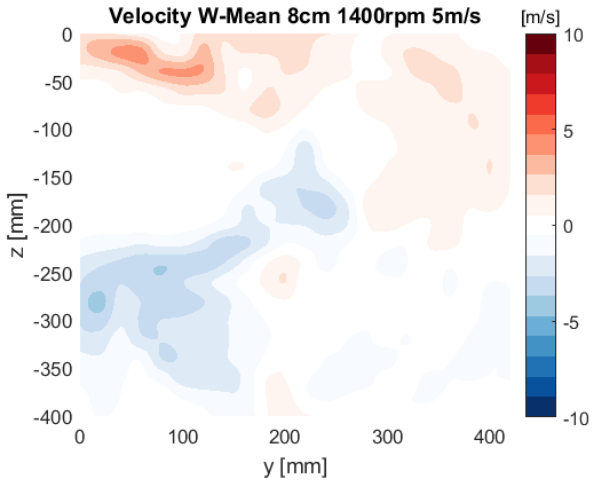

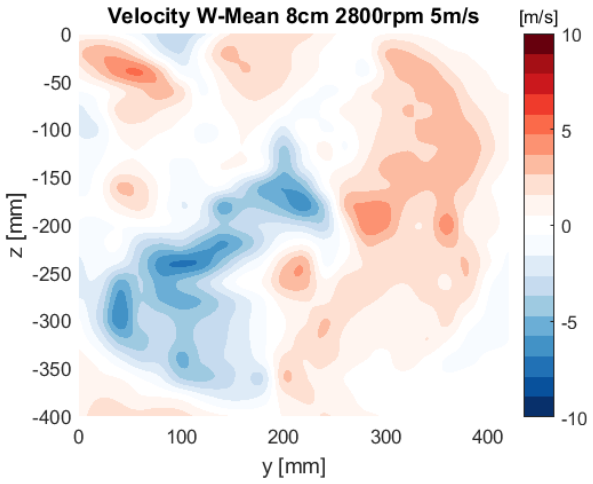

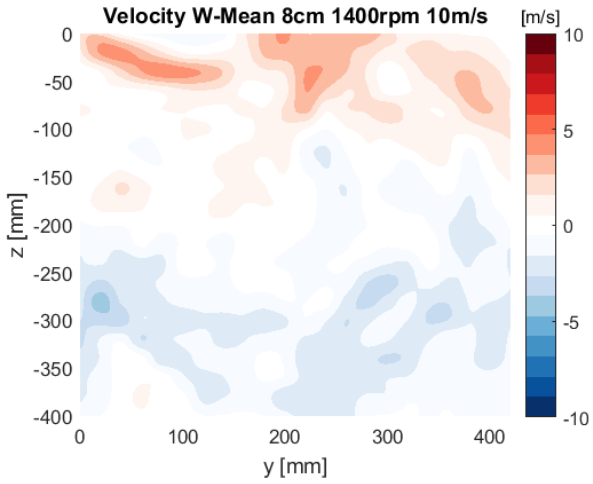

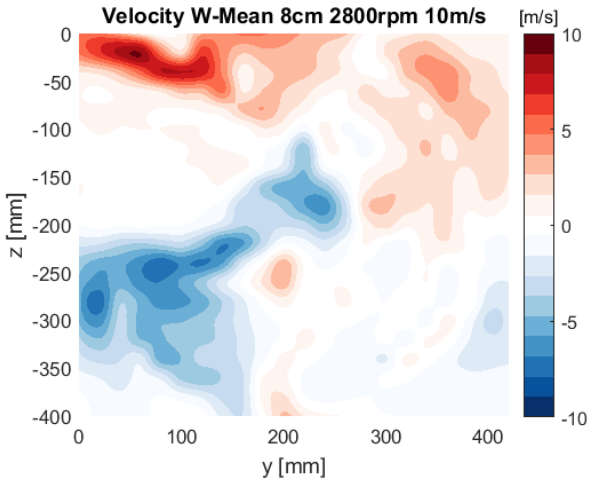

12cm Downstrean

Streamwise

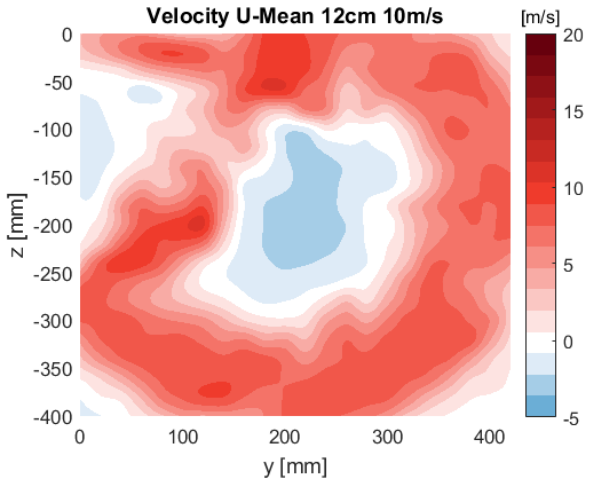

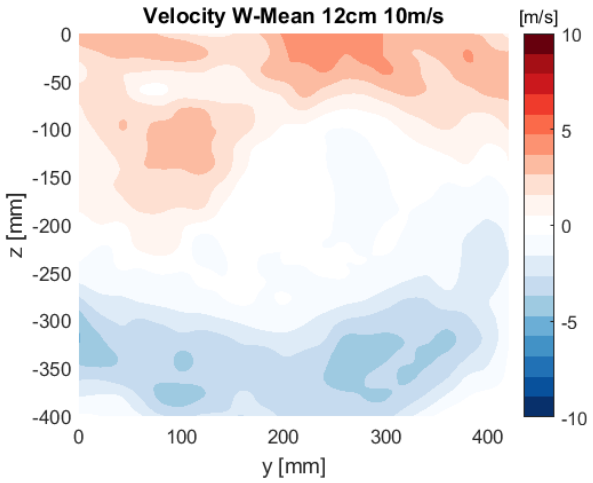

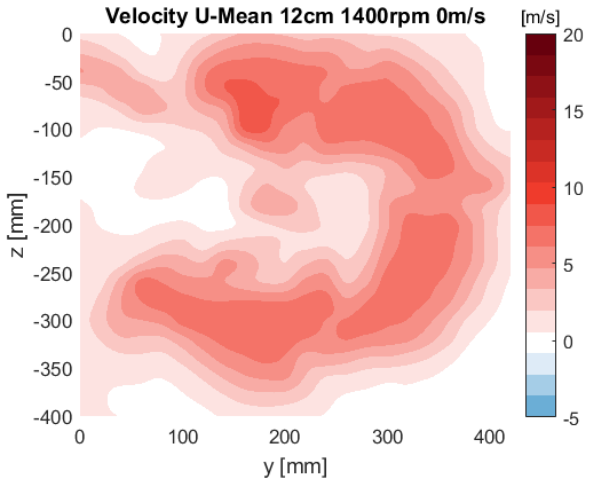
Velocity U-Mean 12cm 1400rpm 0m/s
[m/s]
z [mm]
y [mm]

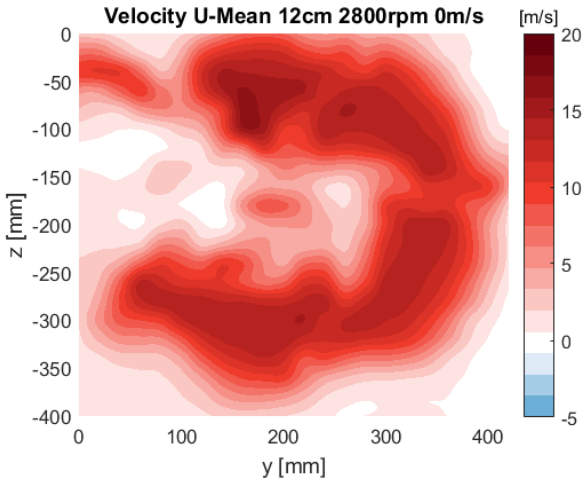
Velocity U-Mean 12cm 2800rpm 0m/s
[m/s]
z [mm]
y [mm]

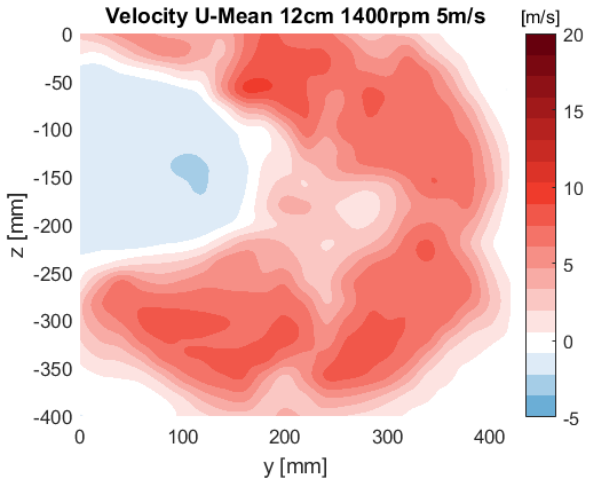
Velocity U-Mean 12cm 1400rpm 5m/s
[m/s]
z [mm]
y [mm]

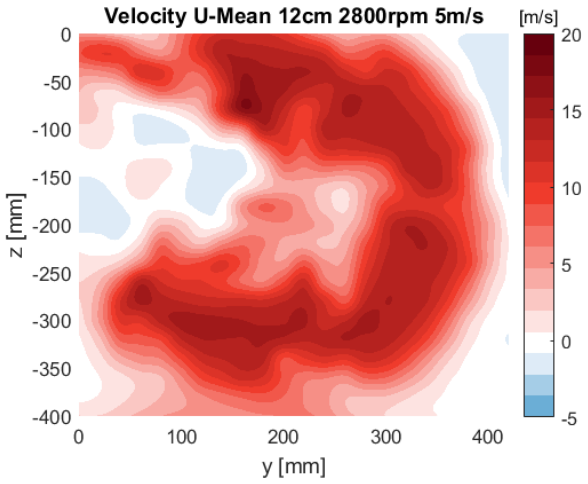
Velocity U-Mean 12cm 2800rpm 5m/s
[m/s]
z [mm]
y [mm]

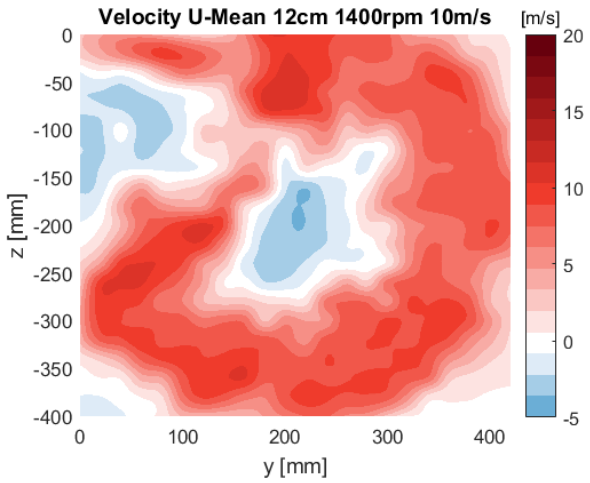
Velocity U-Mean 12cm 1400rpm 10m/s
[m/s]
z [mm]
y [mm]

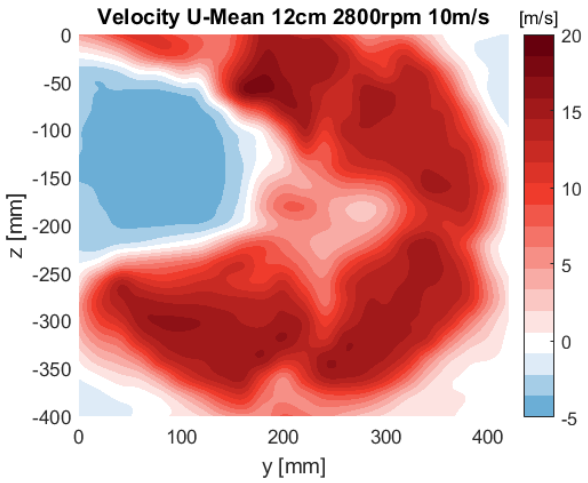
Velocity U-Mean 12cm 2800rpm 10m/s
[m/s]
z [mm]
y [mm]

Vertical Cross-Stream

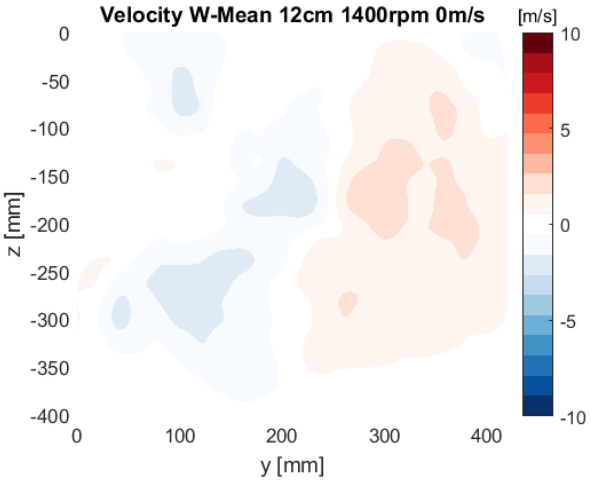

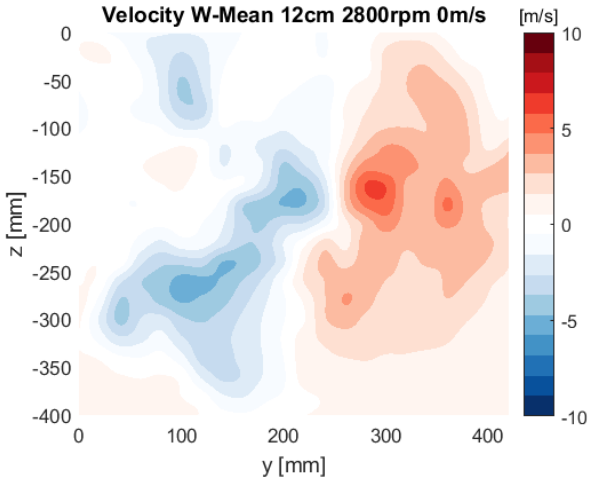

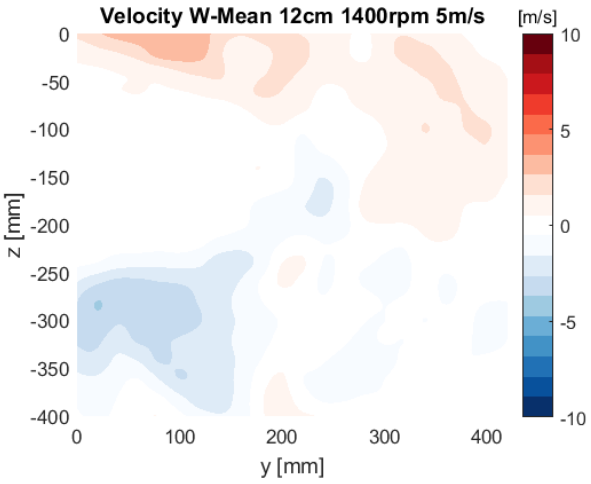

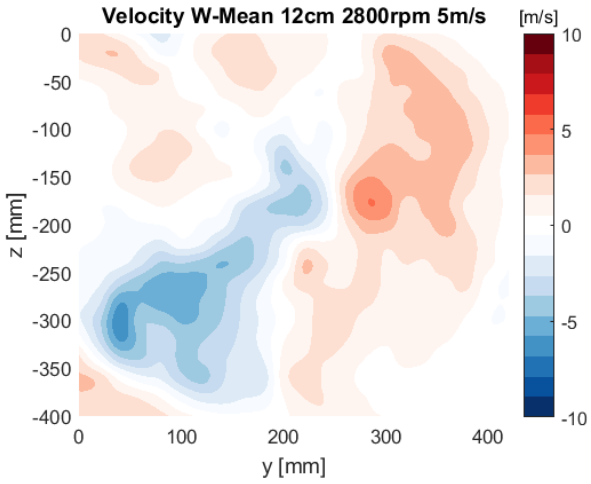

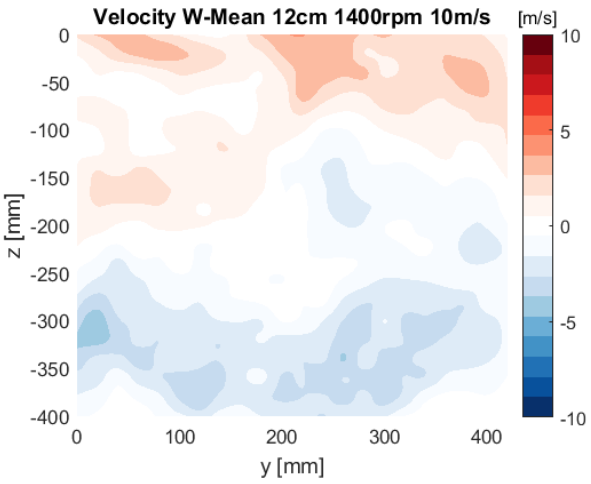

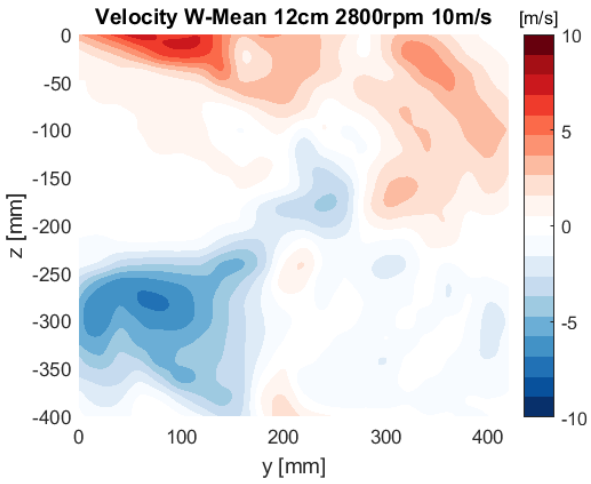

B Appendix

In Appendix 2 it is shown how the freestream wind tunnel velocity in streamwise direction varies in the centre of the tunnel. The measurements were performed at test section, approximately 80 cm downstream of the boundary layer suction and four different wind velocities (3, 5, 10 and 20 m/s) were tested. Boundary layer suction were used for all tests. The plots show measurements repeated 150 times at the same position, even distributed during approximately 30 minutes.

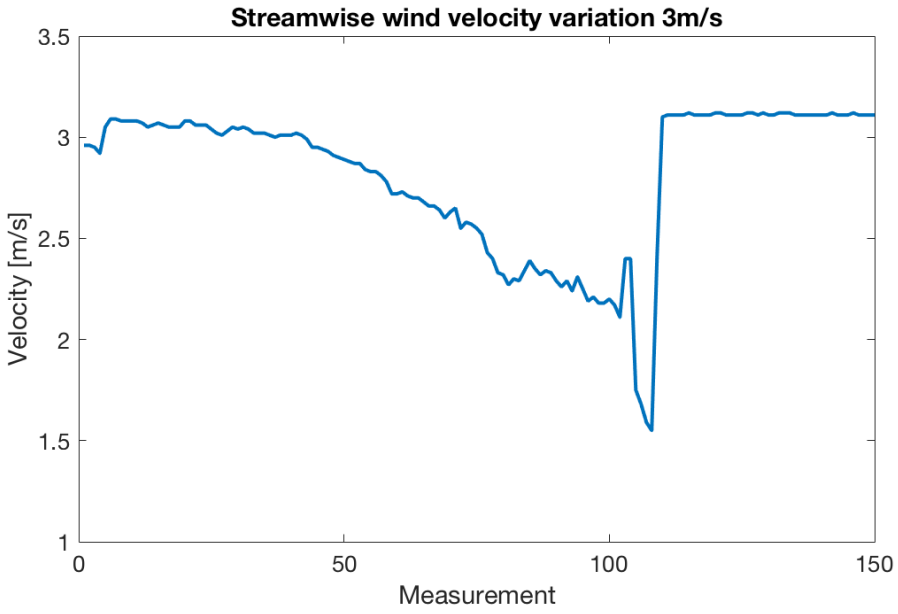

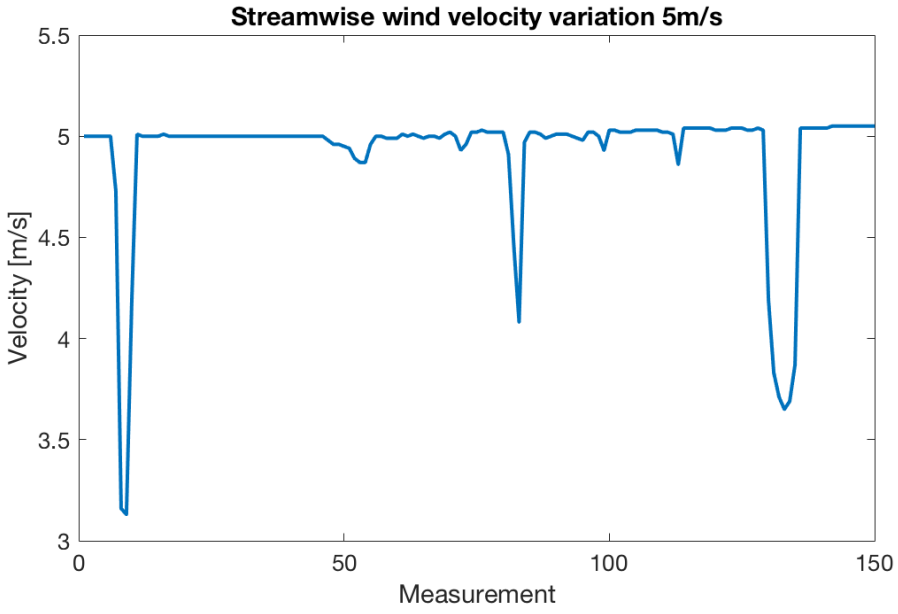

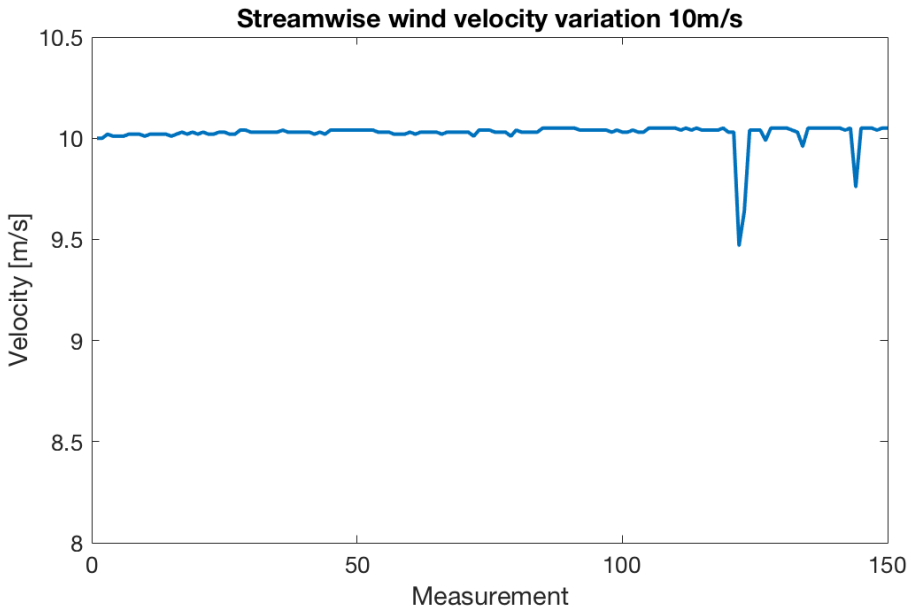
Streamwise wind velocity variation 10m/s
10.5
10
9.5
9
8.5
8
Velocity [m/s]
0
50
100
150
Measurement

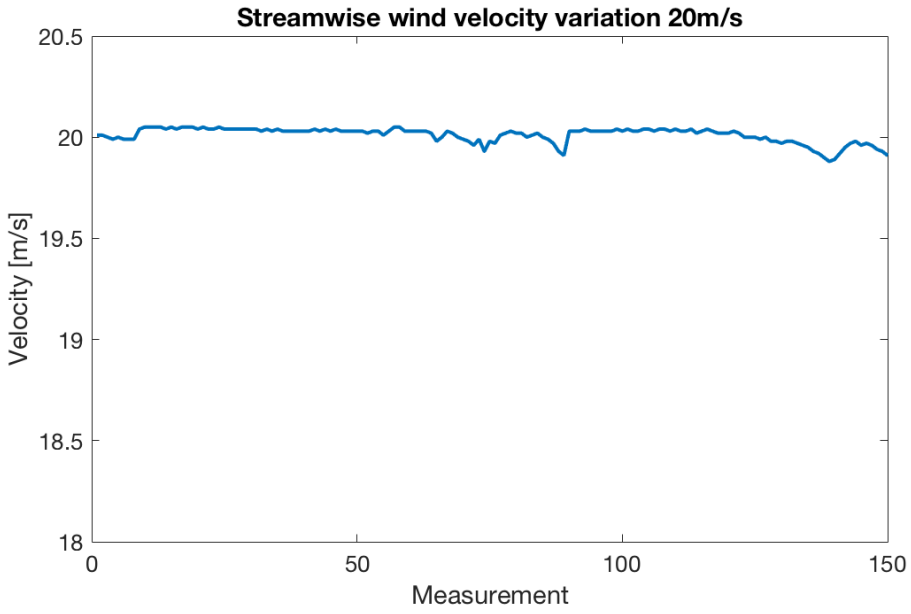
Streamwise wind velocity variation 20m/s
20.5
20
19.5
19
18.5
18
Velocity [m/s]
0
50
100
150
Measurement